SUBSTITUTION EFFECTS OF PHENOTHIAZINE AND PORPHYRIN DYES IN DYE-SENSITIZED SOLAR CELLS

Aaron S. Hart, B.S.

Thesis Prepared for the Degree of

MASTER OF SCIENCE

UNIVERSITY OF NORTH TEXAS

December 2013

APPROVED:

Francis D'Souza, Major Professor
Justin Youngblood, Committee Member
William E. Acree, Jr., Committee Member and Chair of the Department of Chemistry
Mark Wardell, Dean of the Toulouse Graduate School

Hart, Aaron S. *Substitution Effects of Phenothiazine and Porphyrin Dyes in Dye-Sensitized Solar Cells.* Master of Science (Chemistry – Analytical Chemistry), December 2013, 87 pp., 5 tables, 25 illustrations, chapter references.

The details of dye sensitized solar cells was explained and phenothiazine and porphyrin based dyes were synthesized for use in DSSCs. DSSCs offer a unique and cost effective method of renewable energy. DSSCs are characterized through various tests, with the overall efficiency, η, bearing the greatest importance. Incident photon to current conversion efficiency, or *IPCE*, is also another important characterization of DSSCs.

Effect of positioning of the cyanoacrylic acid anchoring group on ring periphery of phenothiazine dye on the performance of dye sensitized solar cells (DSSCs) is reported. The performances of the cells are found to be prominent for solar cells made out of Type-1 dyes compared to Type-2 dyes. This trend has been rationalized based on spectral, electrochemical, computational and electrochemical impedance spectroscopy results.

Free-base and zinc porphyrins bearing a carboxyl anchoring group at the *para*, *meta*, or *ortho* positions of one of the *meso*-phenyl rings were synthesized for DSSCs. Photoelectrochemical studies were performed after immobilization of porphyrins onto nanocrystalline TiO_2. The performance of DSSCs with the porphyrin anchoring at the *para* or *meta* position were found to greatly exceed those in the *ortho* position. Additionally, zinc porphyrin derivatives outperformed the free-base porphyrin analogs, including better dye regeneration efficiency for the zinc porphyrin derivatives and for the *meta* and *para* derivatives through electrochemical impedance spectroscopy studies. The overall structure-performance trends observed for the present porphyrin DSSCs have been rationalized based on spectral, electrochemical, electrochemical impedance spectroscopy and transient spectroscopy results.

ACKNOWLEDGEMENTS

I would like to thank Dr. Navaneetha K. Subaiyyan for the knowledge and training received in making solar cells, Chandra KC, for synthesizing the phenothiazine and porphyrin compounds described in the second and third chapters of this thesis, Habtom Gobeze, for collecting and interpreting the transient spectroscopy data mentioned in the third chapter, Dr. Paul Karr of Wayne State College, for performing the theoretical computations in the second chapter, NSF Grant No. 1110942, for funding this research, and Dr. Francis D'Souza, committee members: Dr. Youngblood and Dr. Acree, and the University of North Texas Department of Chemistry for giving me the opportunity to perform and present this research.

TABLE OF CONTENTS

CHAPTER 1

INTRODUCTION TO DYE-SENSITIZED SOLAR CELLS

1.1) Why Study Solar Cells?

With the rapid decline in the supply of fossil fuel resources, research has been highly motivated toward renewable energy. One potential replacement for fossil fuels is solar energy. This idea is based largely on the chlorophyll pigments found in the cells of leafs in plants and used for photosynthesis. Solar cells work by taking sunlight and converting them into current, unlike glucose and oxygen in natural photosynthesis, which is then distributed, as seen in Figure 1.1. However, much like in plants, a lone solar cell is not sufficient enough for use in this manner so they are used in a grid formation. Solar cells come in many different types such as crystalline silicon, organic, and dye-sensitized solar cells (DSSC). Thus far, crystalline silicon solar cells offer the highest quantum efficiency, $\eta = 25\%$, as a single junction cell; however, they are limited by the use of expensive crystalline silicon as the medium for charge injection. DSSCs offer the most economical and efficient solution due to their use of cheaper materials.[1-2]

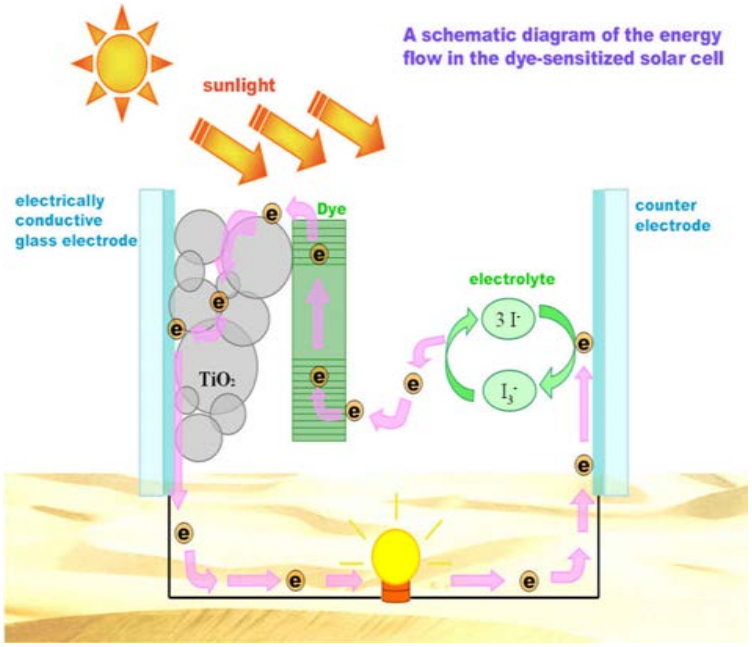

Figure 1.1: Basic scheme showing electron injection in dye-sensitized solar cells (DSSCs) taken from DeepResource (http://deepresource.wordpress.com/2012/05/12/solar-power-to-dye-for/).

A wide range of organic molecules can be used as dyes in DSSCs, such as porphyrins[3-9], pthalocyanines[10-11], coumarin[12], phenothiazine[13-16], carbon nanotubes[17-20], and quantum dots[21-24]. In 1991, Michael Grätzel and Brian O'Regan revolutionized solar cell technology by fully characterizing a novel dye, N3, was which they synthesized and showed to have a quantum efficiency of 7%,[1] where it would be the highest performing dye for nearly a decade. In 1998, N719, another ruthenium derivative, was synthesized and shown to be the first sensitizer dye to reach double digit efficiency at ~10-11%.[2][25] Not only did quantum efficiency increase, but also the incident photon to current conversion efficiency, or IPCE, improved to 80% and the spectral coverage included 100 nm further into the infrared region.[2] More recently, a porphyrin-based DSSC was reported of having an efficiency of 12.1%; this is the currently the highest reported efficiency.[26]

1.2) The Limitations of Solar Cells

The application of solar cells is limited thermodynamically by the Carnot cycle, or rather the Carnot engine. This limits the maximum efficiency between 93-95%, due to the first and second laws of thermodynamics. Furthermore, ideal solar cells operating at one sunlight intensity are limited to a maximum efficiency of 31% through the following conditions: a) graphical analyses displaying the magnitude of loss, b) multiple and single energy gaps considered, c) a terrestrial solar spectrum, d) the effect of concentrated sunlight, e) the thermodynamic limit to solar energy conversion; and is represented in Figure 1.2.[27]

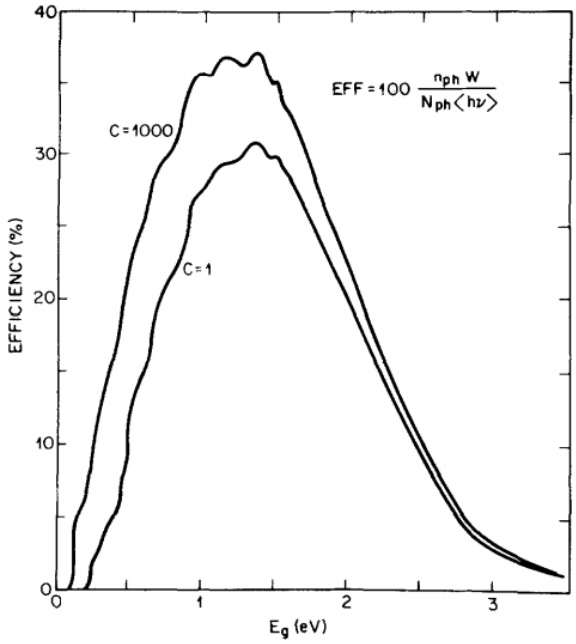

Figure 1.2: Solar cell efficiency as a function of energy gap for concentrations, C = 1 sunlight and C = 1000 suns.[27]

In addition to that, the efficiency is further limited by the various pathways in which the electron, created by the incident photon from the sun, can travel. One possibility is that the photon was of

insufficient energy and so the electron recombines with the generated hole, leaving no net current generated.[28] There is also dark current, which is the main channel of energy loss in solar cells. Dark current in solar cell junctions flows in the direction opposite of the current generated by light excitation and is caused by back recombination from the oxide film to I_3^- mediator.[29] Lastly, the best pathway, at least in terms of current generation, leads to excitation of the electron into the LUMO followed by injection into the film interface. The electron then passes through a device which is able to harness the current generated before the electron returns to the cell interface through the counter electrode.

1.3) Flow of Electrons in DSSC

In DSSCs, a photon enters the cell via light illumination, resulting in excitation of a photosensitizer, S, absorbed on the surface of an oxide film mounted to a glass substrate. The electron from the excited state, S*, is then injected into the oxide film and transferred to the FTO glass substrate. It is possible that at this point that the electron could be returned to film via back recombination, however, the surface area of the oxide film is much greater than that of the substrate, making this back electron transfer negligible. Decay from S* to S is also possible.[28] In order to keep this minimized, the rate of charge injection, K_{inj}, must be greater than that of the rate of decay for the dye. The electron is then regenerated in the dye by use of a redox mediator solution, typically I^-/I_3^-.[29]

Addition of 4-t-butylpyridine has been shown to improve the performance of the I^-/I_3^- mediator by raising the potential of the conduction band and also reducing recombination phenomena, resulting in improved DSSC characteristics.[30] Another common redox mediator is Co(II)/Co(III) can be substituted for the iodine couple when using porphyrin based dyes.

However, this redox couple can negatively affect the performance of the dye, as the potential and current values obtained are often lower.[31] Yum et al. reported that the same redox coupled showed success when used with molecule Y123 prepared on TiO_2 substrate, resulting in increased efficiency as a result of greater potential values, while only losing a small amount of current and obtaining an efficiency of about 10%.[32] Recent studies on the Br^-/Br_3^- redox couple have shown an increase in the open circuit potential at the cost of some current, yet still yielding a higher efficiency in some cases.[33]

1.4) Choosing an Oxide Film Substrate

Typically, films in DSSCs share similar properties as semiconductor films. There are two types of films for application in DSSCs: n-type and p-type. They work in similar fashion as their semiconductor counterparts; n-type films depend on the generation of electrons for current and p-type films depend on the recombination of holes to generate current. Examples of n-type films for DSSC practices include TiO_2, SnO_2,[34-39] and ZnO[40-42]. Conversely, NiO represents one of the only well studied p-type films.[43-45] TiO_2 has shown the highest solar conversion efficiency of any semiconductor film material.

Titania, the common name for TiO_2, has distinct advantages as a DSSC film in that it is a cheap material, widely available, non-toxic, and most importantly, it does not absorb light throughout most of the visible light spectrum. Anatase TiO_2 is the most commonly used form in DSSCs as opposed to rutile titania. The band gap for anatase is 3.2 eV is more favorable for these purposes, as opposed to the band gap for rutile material which is 3.0 eV.[46] It is usually screen printed[29, 47] or applied via the "doctor blade" technique[48-49] leaving it as a film after

annealing. This form is less preferential as opposed to single crystal TiO_2 as the back combination of electrons with redox solution leads to major losses in energy via dark current.[29]

The use of $TiCl_4$ to treat the FTO before and after applying the TiO_2 film has been shown to improve the overall efficiency of the DSSCs. Essentially with each treatment, a small layer of TiO_2 is annealed to the substrate surface. The first treatment of FTO with $TiCl_4$ in H_2O strengthens the bond between the smooth FTO substrate and the applied TiO_2 layer. It also helps block recombination from the SnO_2 on the surface of FTO to the holes in redox mediator solution. A second treatment following application and annealing of the TiO_2 film enhances the roughness of the film surface. After annealing, the nanoparticles in the film become very compact and smooth. By roughing up the surface, more dye sensitizer is allowed to bond to the film surface.[29]

Zhao et al. found that the temperature at which the film is annealed also can affect the efficiency. The authors studied the efficiency of DSSCs using homemade titania and annealing each film at temperatures ranging from 350° C to 600° C. The authors found that generally the higher annealing temperature yielded better results. However, the mesoporous structure of the film was lost when annealing at 600° C, leading them to conclude that 500° C worked the best, as it maintained the mesoporous structure, resulting in a higher efficiency. This conclusion was also supported by electrochemical impedance spectroscopy data.[49]

1.5) Building an Ideal Sensitizer Molecule

Building an ideal sensitizer starts with anchoring the molecule to the oxide film surface. Most commonly, carboxylate groups are used for anchoring, but some have also used phosphonate groups, such as those found in the ruthenium based dyes.[1][2] Next, the dye

molecule must have a wide absorption range under visible light. This is a common obstacle when using molecules such as porphyrins and phthalocyanines as neither dye exhibits full coverage of the visible spectrum. However, by coupling the two as co-absorbers, the DSSC are able to utilize more of the spectrum.[39, 50] The energy level of the excited state of the dye should be matched with the lower boundaries of the conduction band of the oxide film in use. This is known to minimize the energetic losses from electron transfer into the film substrate. The redox potential of the sensitizer molecule must also be relatively high, or rather not too easily oxidized or reduced, so as to facilitate regeneration. Perhaps, the most overlooked quality of an ideal dye is that they need to be stable, generally last 10^8 turnover cycles, before they can be applied practically.[29]

The rate at which the excited dye injects the electron into the TiO_2 substrate is also of some importance. The lifetime of the injected electron should be fairly quick, in the femtosecond to picosecond time scale. However, the rate of injection, k_{inj}, should be slower than the rate of decay in the dye. Similarly, dye cation decay must occur at a slower rate than the rate of reduction by iodide.[29]

Absorbing molecules in solution with the sensitizer, the previously mentioned co-absorbers, has been shown to improve the efficiency of DSSCs.[51-52] Commonly, compounds with their own anchoring group, such as chenodeoxycholic acid (CDCA), have been employed with sensitizers. Using these compounds, researchers have been able to increase the efficiency of N719, a ruthenium-based dye, up to 12%, a 20% increase over the efficiency of the dye alone.[26] Jing et al. reported the use of CDCA with phenothiazine as the sensitizer, resulting in lower dye concentration with the co-absorber yet increased current, demonstrating that CDCA

helps dissociate aggregates formed in solution.[52] Parasullo et al, reported a seven-fold increase in the photoactivity by coordinating porphyrin molecules with ruthenium bipyridyl complexes.[9]

1.6) Counter Electrode Materials and Preparation

The last component of the DSSC setup is the counter electrode. The counter electrode should be made from a material that exhibits good electrocatalytic properties. Platinum is a commonly used material because it shows good stability as well as possessing a low overpotential. Perhaps one of the less time consuming methods, Papageorgiou et al. reports a method of coating FTO glass substrate via the thermal decomposition of chloroplatinic acid, H_2PtCl_6, they showed that the thermally deposited Pt is superior to electrochemically deposited Pt, due the inability of the latter method to reduce iodine.[53] Others have explored more organic methods, to reduce the cost of materials. Murakami et al. reported using carbon paste on FTO, resulting in an efficiency greater than 9%, a record for carbon based DSSC. [54] Lee et al. reported using nanoscale carbon powders and carbon nanotubes with some success.[55] Similarly, Kamat et al. explored using graphene oxide-Cu_2S as a counter electrode, finding that the application more than doubled the efficiency of their quantum dot solar cells.[56]

1.7) Characterization of DSSCs

Characterization of DSSCs begins with quantum, or overall, efficiency expressed as η. Eta can be calculated by Equation 1.1:[29]

$$\eta = \frac{I_{sc} \cdot V_{oc} \cdot FF}{P_{in}} \qquad \text{(Equation 1.1)}$$

where I_{sc} is the short circuit current, V_{oc} is the open-circuit potential, P_{in} is the incident power, and *FF* is the fill factor which is the defined as the ratio of the maximum power divided by the product of I_{sc} and V_{oc}. The short-circuit current defines the interaction between the oxide film and the sensitizer. A large value for I_{sc} could be due to three occurrences: 1) intense light absorption by the sensitizer over a wide spectrum of visible light, 2) high electron injection efficiency from sensitizer to the conduction band of TiO_2, and 3) efficient reduction of oxidized dye by the iodide ion. V_{oc} represents the difference in energy level between the CB of oxide and the redox potential of the mediator solution. This value is limited by dark current, formed by the back reaction previously described.[57] P_{in} is typically set to 100 mW cm^{-2}, as defined by one sunlight irradiation. The quantum efficiency is obtained by measuring current while sweeping a potential range under light irradiation, thus obtaining an *I-V* curve.[29] The relationship between this curve and the above described values can be seen in Figure 1.3.

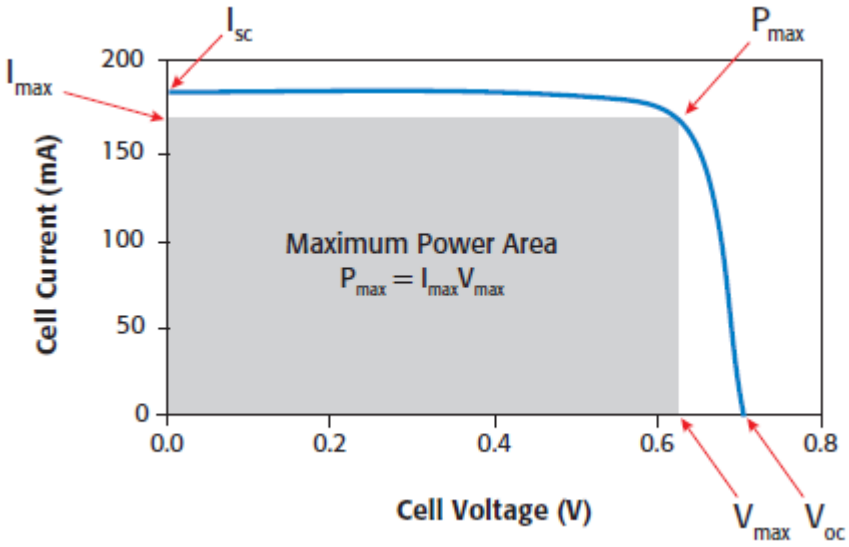

Figure 1.3: Properties extrapolated from a typical I-V curve for use in DSSCs from Keithley Instruments, Inc.[61]

Another value that characterizes the capabilities of a dye sensitizer to convert sunlight into energy is the incident photon to current conversion efficiency (IPCE). IPCE shares a direct relationship with the absorption spectrum of the dye sensitizer. IPCE represents the efficiency in which electrons on collected in the assembled solar cell circuit and is determined by Equation 1.2:[29]

$$IPCE(\%) = \frac{I_{sc}(A)}{P(W)} \times \frac{1240}{\lambda(nm)} \times 100 \qquad \text{(Equation 1.2)}$$

IPCE is measured by collecting current while varying the wavelength of light illuminating the dye sensitizer. As seen by the equation, a large value for I_{sc} leads directly to a greater percentage for IPCE. The maximum IPCE values experimentally possible are in the 85-90% percent range, due to absorption of the light by the FTO glass substrate.[29]

The stability of DSSCs can be characterized by two methods: current switching and photovoltage decay. In current switching, the cell is irradiated by light for known intervals of time, showing the stability of the current produced. If the sensitizer is stable, then it would produce similar current values for each time irradiated by light. Photovoltage decay can be an effective tool in testing the effectiveness of the blocking layer between the film and FTO substrate. It can also be a useful tool in determining the electron lifetime in terms of charge injection.[40, 67] Patterson et al. showed stability of 180 days for dye operating under low light conditions (~5000 lux, or about 15% of direct sunlight).[29]

Electrochemical impedance spectroscopy (EIS) can be helpful in characterizing the simultaneous electron transport to the TiO_2 and electron transfer in the back reaction. By using EIS, DSSCs can be modeled with an equivalent circuit, as they are most basically a simple circuit. The experiment works by scanning a range of frequencies, while applying a constant potential. The data obtained for DSSCs is usually modeled in the form of a Nyquist plot. A

typical Nyquist plot, a plot of both real and imaginary resistances, consists of at least two semicircles representing: 1) the resistance of the platinum counter electrode, R_{Pt}, found in the high frequency region and 2) charge transfer resistance of the oxide layer, R_{CT}, found in the intermediate region of the frequency range.[83] Values for R_{CT} should be lower for data collection under light illumination when compared to same cell in darkness. Ignoring recombination losses, this may be attributed to an increased concentration of I_3^- near the interface of the dyed oxide film due to the regeneration of dye molecules.[83] This can also be attributed to the decreased viscosity of the mediator solution as a result of the elevated temperature of the solution under illumination.[12] EIS studies performed by Kwon et al. have shown a standard dye, N719, to have a charge transfer resistance of 290 Ω/cm^2 with a film 8 μm thick and 1540 Ω/cm^2 with a film 2 μm thick under illumination.[84]

1.8) Conclusion

The following chapters will discuss the performance of derivatives of phenothiazine and porphyrin dyes in Grätzel cell DSSCs. In the case of phenothiazine dyes, the position of the cyanocinnamic acid group was probed in both the C-3 and N-terminal positions. In the case of the porphyrin derivatives, the effect of zinc metallation was examined. In addition, the position of carboxylic acid functional group in the para, meta, and ortho positions on the meso-phenyl ring was also studied. Photoelectrochemical and EIS studies were performed on both sets of dyes. Additional studies on femtosecond transient spectroscopy were performed in the case of the porphyrin derivatives.

1.9) References

1. O'Regan, B.; Grätzel, M. *Nature*, **1991**, *353*, 737.
2. Kalyanasundaram, K.; Grätzel, M. *Coord. Chem. Rev.* **1998**, *77*, 347.
3. Wu, S-L.; Lu, H.-P.; Yu, H.-T.; Chuang, S.-H.; Chiu, C.-L.; Lee, C. W.; Diau, E. W.-G.; Yeh, C.-Y. *Energy and Environ. Sci*. **2010**, *3*, 949.
4. Lee, C. Y.; Hupp. J. T. *Langmuir*, **2010**, *26*, 3760.
5. Kamat, P. V. *J. Phys. Chem. C*, **2007**, *111*, 2834.
6. Umeyama T.; Imahori, H. *Energy Environ. Sci.*, **2008**, *1*, 120.
7. Hasobe, T. *Phys. Chem. Chem. Phys.*, **2010**, *12*, 44.
8. Subbaiyan, N. K.; Wijesinghe, C. A.; D'Souza, F. *J. Am. Chem. Soc*., **2009**, *131*, 14646.
9. Parussulo, A. L. A.; Iglesias, B. A.; Toma, H. E.; Araki, K. *Chem. Commun*. **2012**, *48*, 6939.
10. Ragoussi, M.-E.; Cid, J.-J. Yum, J.-H.; de la Torre, G.; Di Censo, D.; Gratzel, M.; Nazeeruddin, M. E.; Torres, T. *Angew. Chem. Int. Ed. Engl*. **2012**, *51*, 4375.
11. Martinez-Diaz, M. V.; de la Torre, G.; Torres, T. *Chem. Commun*. **2010**, *46*, 7090.
12. Wang, Z. S.; Cui, Y.; Dan-oh, Y.; Kasada, C.; Shinpo, A.; Hara, K.; *J. Phys. Chem. C*, **2007**, *111*, 7224.
13. Tian, H.; Yang, X.; Chen, R.; Pan, Y.; Li, L.; Hagfeldt, A.; Sun, L. *Chem. Commun.*, **2007**, 3741.
14. Cao, D.; Peng, J.; Hong, Y.; Fang, X.; Wang, L.; Meier, H. *Org. Lett.*, 2011, **13**, 1610 .
15. Xie, Z.; Midya, A.; Loh, K. P.; Adams, S.; Blackwood, D. J.; Wang, J.; Zhang, X.; Chen, Z. *Prog. Photovoltaics*, **2010**, *18*, 573.
16. Wu, W.; Yang, J.; Hua, J.; Tang, J.; Zhang, L.; Long, Y.; Tian, H. *J. Mater. Chem.*, **2010**, *20*, 1772.

17. D'Souza, F.; Ito, O. *Chem. Soc. Rev*. **2012**, *41*, 86.

18. D'Souza, F.; Sandanayaka, A. S. D.; Ito, O. *J. Phys. Chem. Letts.* **2010**, *1*, 2586.

19. Kamat P. V.; Schatz, G. C. *J. Phys. Chem. C*, **2009**, *113*, 15473.

20. Rochford, J.; Chu, D.; Hagfeldt, A.; Galoppini, E. *J. Am. Chem. Soc.* **2007**, *129*, 4655.

21. Sargent, E. H.; *Nature Photonics*, **2012**, *6*, 133.

22. Bang, J. H.; Kamat, P. V. *ACS Nano*, **2009**, *3*, 1467.

23. Tang, J.; Wang, X.; Brzozowski, L.; Barkhouse, D.; Aaron, R.; Debnath, R.; Levina, L.; Sargent, E. H. *Adv. Mater*. **2010**, *22*, 1398.

24. Santra, P. K.; Kamat, P.V. *J. Amer. Chem. Soc.* **2013**, *135*, 877.

25. Yum, J-H.; Moon, S-J.; Kathikeyan C. S.; Wietasch, H.; Thelakkat, M.; Zakeeruddin, S. M.; Nazeeruddin, M. K., Grätzel, M. *Nano Energy* **2012**, *1*, 6.

26. Yella, A.; Lee, H-W.; Tsao, H. N.; Yi, C.; Chandiran, A. K.; Nazeeruddin, M. K.; Diau, E. W.; Yeh, C-Y.; Zakeeruddin, S. M.; Grätzel, M. *Science* **2011**, *334*, 629.

27. Henry, C. H. *J. Appl. Phys.* **1980**, *51*, 4494.

28. Ooyama, Y.; Harima, Y. *Eur. J. Org. Chem.* **2009**, 2903.

29. *Dye-Sensitized Solar Cells*, Ed. Kalyanasundaram, EPFL Press, Lausanne, 2010.

30. Nazeeruddin, M. K.; Kay, A.; Rodico, I.; Humphry-Baker, R.; Muller, E.; Lisk, P.; Valchopoulos, N.; Grätzel, M. *J. Am. Chem. Soc.* **1993**, *115*, 6382.

31. Liu, Y.; Jennings, J. R.; Huang, Y.; Wang, Q.; Zakeeruddin, S. M.; Grätzel, M. *J. Phys. Chem. C* **2011**, *115*, 18847.

32. Yum, J-H.; Baranoff, E.; Kessler, F.; Moehl, T.; Ahmad, S.; Bessho, T; Marchioro, A.; Ghadiri, E.; Moser, J-E.; Yi, C.; Nazeeruddin, M, K.; Grätzel, M. *Nature Communications* **2012**, 1.

33. Wang, Z-S.; Sayama, K.; Sugihara, H. *J. Phys. Chem. B* **2005**, *109*, 22449.

34. Bedja, I.; Hotchandani, S.; Kamat, P. V. *J. Phys. Chem.* **1994**, *98*, 4133.

35. Liu, D.; Fessenden, R. W.; Hug, G. L.; Kamat, P.V. *J. Phys. Chem. B* **1997**, *101*, 2583.

36. Hasobe, T.; Saito, K.; Kamat, P. V.; Troiani, V.; Qiu, H.; Solladie, N.; Kim, K. S.; Park, J. K.; Kim, D.; D'Souza, F.; Fukuzumi, S. *J. Mater. Chem.* **2007**, *17*, 4160.

37. Subbaiyan, N. K.; Maligaspe, E.; D'Souza, F. *ACS Appl. Mater. Interfaces* **2011**, *3*, 2368.

38. Shang, G.; Wu, J.; Huang, M.; Lin, J.; Lan, Z.; Huang, Y.; Fan, L. *J. Phys. Chem. C* **2012**, *116*, 20140.

39. Subbaiyan, N. K.; D'Souza, F. *Chem. Comm.* **2012**, *48*, 3641.

40. Wang, J. X.; Wu, C. M. L.; Cheung, W. S.; Luo, B.; He, Z. B.; Yuan, G. D.; Zhang, W. J.; Lee, C. S.; Lee, S. T. *J. Phys. Chem. C* **2010**, *114*, 13157.

41. Qiu, J.; Guo, M.; Wang, X.; *ACS Appl. Mater. Interfaces* **2011**, *3*, 2358.

42. Gnitchwitz, J-K.; Marczak, R.; Werner, F.; Lang, N.; Jux, N.; Guldi, D. M.; Peukert, W.; Hirsch, A. *J. Am. Chem. Soc.* **2010**, *132*, 17910.

43. Boschloo, G.; Hagfeldt, A. *J. Phys. Chem. B* **2001**, *105*, 3039.

44. Nattestad, A.; Ferguson, M.; Kerr, R.; Cheng, Y-B. *Nanotechnology* **2008**, *19*, 29503.

45. Lepleux, L.; Chavillon, B.; Pellegrin, Y.; Blart, E.; Cario, L.; Jobic, S.; Odobel, F. *Inorg. Chem.* **2009**, *48*, 8245.

46. Kamat, P. V. *J. Phys Chem. C* **2012**, *116*, 11849.

47. Ito, S.; Murakami, T. N.; Comte, P.; Liska, P.; Grätzel, C; Nazeeruddin, M. K.; Grätzel, M. *Thin Solid Films* **2008**, *516*, 4613.

48. Kontos, A. I.; Kontos, A. G.; Tsoukleris, D. S.; Bernard, M-S.; Spyrellis, N.; Falaris, P. *J. Mater. Processing Technology* **2008**, *196*, 243.

49. Zhao, D.; Peng, T.; Lu, L.; Cai, P.; Jiang, P; Bian, Z. *J. Phys Chem. C* **2008**, *112*, 8486.

50. Martinez-Diaz, M. V.; de la Torre, G.; Torres, T. *Chem. Comm.* **2010**, *46*, 7090.

51. Han, L.; Islam, A.; Chen, H.; Malapaka, C.; Chiranjeevi, B.; Zhang, S.; Yang, X.; Yanagida, M. *Energy Environ. Sci.* **2012**, *5*, 6057.

52. Li, J.; Wu, W.; Yang, J.; Tang, J.; Long, Y.; Hua, J. *Science China* **2011**, *54*, 699.

53. Papageorgiou, N.; Maier, W. F.; Grätzel, M. *J. Electrochem. Soc.* **1997**, *144*, 876.

54. Murakami, T.; Ito, S.; Wang, Q.; Nazeeruddin, M. K.; Bessho, T.; Cesar, I.; Liska, P.; Humphry-Baker, R.; Comte, P.; Péchy, P.; Grätzel, M. *J. Electrochem. Soc.* **2006**, *153*, A2255.

55. Lee, W. J.; Ramasamy, E.; Lee, D. Y.; Song, J. S. *ACS Appl. Mater. Interfaces Letters* **2009**, *1*, 1145.

56. Radich, J. G.; Dwyer, R.; Kamat, P. V. *J. Phys. Chem. Letters* **2011**, *2*, 2455.

57. Mishra, A.; Fischer, M. K. R.; Bäuerle, P. *Angew. Chem. Int. Ed.* **2009**, *48*, 2478.

58. Chen, S.; Xu, X.; Liu, Y.; Yu, G.; Sun, X.; Qiu, W.; Ma, Y.; Zhu, D. *Adv. Funct. Mater.*, **2005**, *15*, 1541.

59. Yoon, K. R.; Ko, S.-O.; Lee, S. M.; Lee, H. *Dyes Pigm.*, **2007**, *75*, 567.

60. Lai, R. Y.; Fabrizio, E. F. Lu, L.; Jenekhe, S. A.; Bard, A. J. *J. Am. Chem. Soc.*, **2001**, *123*, 9112.

61. Keithley Instruments. Keithley Survey Shows Differing Test Priorities and Methods for Testing Solar Cell/PV Devices (White Paper). www.keithley.com/data?asset=52794 (Accessed 6/11/13).

62. Tsai, Y.-L.; Chang, C.-C.; Kang, C.-C.; Chang, T.-C. *J. Lumin.*, **2007**, *127*, 41.

63. Roquet, S.; Cravino, A.; Leriche, P.; Alévêque, O.; Frère, P.; Roncali, J. *J. Am. Chem. Soc.*, **2006**, *128*, 3459.

64. Mishra, A.; Fischer, M. K. R.; Bäuerle, P. *Angew. Chem., Int. Ed.*, **2009**, *48*, 2474.

65. Hara, K.; Kurashige, M.; Ito, S.; Shinpo, A.; Suga, S.; Sayama, K.; Arakawa, H. *Chem. Commun.*, **2003**, 252.

66. Kitamura, T.; Ikeda, M.; Shigaki, K.; Inoue, T.; Anderson, N. A.; Ai, X.; Lian, T.; Yanagida, S. *Chem. Mater.*, **2004**, *16*, 1806.

67. Zaban, A.; Greenshtein, M.; Bisquert, J. *Chem. Phys. Chem.* **2003**, *4*, 859.

68. Hara, K.; Sato, T.; Katoh, R.; Furube, A.; Yoshihara, T.; Murai, M.; Kurashige, M.; Ito, S.; Suga, S.; Arakawa, H. *Adv. Funct. Mater.*, **2005**, *15*, 246.

69. Xu, W.; Peng, B.; Chen, J.; Liang, M.; Cai, F. *J. Phys. Chem. C*, **2008**, *112*, 874.

70. Liu, W.-H.; Wu, I. C.; Lai, C.-H.; Lai, C.-H.; Chou, P.-T.; Li, Y.-T.; Chen, C.-L.; Hsu, Y.-Y. Chi, Y. *Chem. Commun.*, **2008**, 5152.

71. Hwang, S.; Lee, J. H.; Park, C.; Lee, H.; Kim, C.; Park, C.; Lee, M.-H.; Lee, W.; Park, J.; Kim, K.; Park, N.-G.; Kim, C. *Chem. Commun.*, **2007**, 4887.

72. Ito, S.; Zakeeruddin, S. M.; Humphry-Baker, R.; Liska, P.; Charvet, R.; Comte, P.; Nazeeruddin, M. K.; Péchy, P.; Takata, M.; Miura, H.; Uchida, S.; Grätzel, M. *Adv. Mater.*, **2006**, *18*, 1202.

73. Ito, S.; Miura, H.; Uchida, S.; Takata, M.; Sumioka, K.; Liska, P.; Comte, P.; Péchy, P.; Grätzel, M. *Chem. Commun.*, **2008**, 5194.

74. Smestad, G. P.; Spiekermann, S.; Kowalik, J.; Grant, C. D.; Schwartzberg, A. D.; Adam, M.; Zhang, J.; Tolbert, L. M.; Moons, E. *Solar Energy Mater. & Solar Cells*, **2003**, *76*, 85-105.

75. Wu, W.; Yang, J.; Hua, J.; Tang, J.; Zhang, L.; Long, Y.; Tian, H. *J. Mater. Chem*. **2010**, *20*, 1772.

76. Wan, Z.; Jia, C.; Duan, Y.; Zhang, J.; Lin, Y.; Shi, Y. *Dye & Pigments*, **2012**, *94*, 150.

77. Xie, Z.; Midya, A.; Loh, K. P.; Adams, S.; Blackwood, D. J.; Wang, J.; Zhang, X.; Chen, Z. *Prog. Photovolt.: Res. Appl*. **2010**, *18*, 573.

78. Marszalek, M.; Nagane, S.; Ichake, A.; Hamphry-Baker, R.; Paul, V.; Zakeeruddin, S. M.; Grätzel, M. *J. Mater. Chem*. **2012**, *22*, 889.

79. Hara, K.; Mori, S. S. *Handbook of Photovoltaic Science and Engineering*, Ed. Luque, A.; Hegedus, John-wley, Chichester, UK, 2011, 642.

80. Xu, T.; Lu, R.; Liu, X.; Zheng, X.; Qui, X.; Zhao, Y. *Org. Letts*. **2007**, *9*, 797.

81. Xu, T.; LU, R.; Liu, X.; Chen, P.; Qui, X.; Zhao, Y. *Eur. J. Org. Chem*. **2008**, 1065.

82. Gaina, L.; Porumb, D.; Silaghi-Dumitrescu, I.; Cristea, C.; Silaghi-Dumitrescu, L.; *Can. J. Chem*. **2010**, *88*, 42.

83. Fabregat-Santiago, F.; Bisquert, J.; Garcia-Belmonte, G.; Boschloo, G.; Hagfeldt, A. *Solar Energy Materials and Solar Cells* **2005**, *87*, 117.

84. Kwon, Y. S.; Song, I.; Lim, J. C.; Siva, A.; Park, T. *ACS Appl. Mater. Interfaces* **2012**, *4*, 3141.

CHAPTER 2

PHENOTHIAZINE SENSITIZED ORGANIC SOLAR CELLS: EFFECT OF DYE ANCHOR GROUP POSITIONING ON THE CELL PERFORMANCE*

2.1. Abstract

Effect of positioning of the cyanoacrylic acid anchoring group on ring periphery of phenothiazine dye on the performance of dye sensitized solar cells (DSSCs) is reported. Two types of dyes, one having substitution on the C-3 aromatic ring (Type-1), and another through the N-terminal (Type-2) have been synthesized for this purpose. Absorption and fluorescence studies have been performed to visualize the effect of substitution pattern on the spectral coverage and electrochemical studies to monitor the tuning of redox levels. B3LYP/6-31G* studies are performed to visualize the frontier orbital location and their significance in charge injection when surface modified on semiconducting TiO_2. New DSSCs have been built on nanocrystalline TiO_2 according to traditional two-electrode Grätzel solar cell setup with a reference cell based on N719 dye for comparison. The lifetime of the adsorbed phenothiazine dye is found to be quenched significantly upon immobilizing on TiO_2 suggesting charge injection from excited dye to semiconducting TiO_2. The performances of the cells are found to be prominent for solar cells made out of Type-1 dyes compared to Type-2 dyes. This trend has

---

* Reproduced in full with permission from Hart, A.S.; KC, C.B.; Subbaiyan, N.K.; Karr, P.A.; D'Souza, F. *ACS Appl. Mater. Interfaces.* **2012**, *4*, 5813.

been rationalized based on spectral, electrochemical, computational and electrochemical impedance spectroscopy results.

2.2. Introduction

Dye-sensitized solar cells (DSSCs) have attracted significant attention as potential low cost replacements to silicon based photovoltaic technology.[1] High performance sensitizers capable of wide-band spectral capture are recognized to be a promising strategy for improving the cost-efficiency of the DSSCs. In this regard, organic photosensitizers are recognized to be ideal replacements for traditionally used, relatively expensive, ruthenium metal complex based sensitizers. The metal free organic dyes have much stronger light-harvesting ability than metal complexes because of their high molar extinction coefficients. The common solar dye-design involves donor connected to an electron acceptor anchoring functionality which allows fine-tuning of optical and electrochemical properties. For donors, dialkylaminophenyl groups,[8–10] coumarins,[11] triphenylamines,[12–14] indoline,[15,16] phenothiazine,[17–20] polythiophene,[21] porphyrin,[22-28] phthalocyanine,[29] and quantum dots[30-32] have been successfully utilized. The choice of electron acceptor anchoring functionality in the design is largely based on cyanoacrylic acid functionality although other electron acceptors such as fullerenes,[24-26] nanotubes,[33-34] and other two-dimensional electron acceptors[35] are being developed and optimized by several research groups. The cyanoacrylic acid functionality largely fulfills the need of an electron acceptor while providing the carboxylic acid group to bind nanocrystalline semiconductor surface.

For efficient design of donor-spacer-acceptor dyes, one of the key issues relates to the positioning of the electron acceptor anchoring group on the macrocycle periphery. The dye-nanoparticle interaction which depends upon the orientation and positioning of the HOMO-

LUMO orbitals for efficient charge injection can be fine-tuned by proper dye-nanoparticle immobilization. For example, in case of porphyrin-TiO_2 solar cells, the positioning of carboxy group on the *meso*-phenyl groups is shown to vary the performance of the solar cell.[36] However, such studies on other high performance dyes are scarce, perhaps due to associated synthetic challenges. In the present study, we have undertaken such a task on a well-known for photoelectrochemical applications, phenothiazine dye,[37-40] and report on the effect of positioning of the cyanoacrylic acid functionality on the dye molecule. For this, we have synthesized two types of dyes, viz., dyes having the substitution at the aromatic ring carbon (Type-1, compounds **1-3** in Scheme 2.1) and a dye with substitution through the hetero N-atom of the macrocycle (Type-2, compound **4** in Scheme 2.1). The phenothiazine dyes contain electron-rich sulfur and nitrogen atoms, have non-planar geometry, and exhibit good thermal and electrochemical stability. For Type-1 dyes, the N-atom of the phenothiazine ring was substituted with a methyl, 2-hydroxyethane, or tris(ethyleneglycol) methyl ether groups to visualize their effect, primarily, on preventing aggregation. Additionally, theoretical calculations using DFT methods have been performed in order to optimize the geometry and to visualize location of the HOMOs and LUMOs. The dyes are then used as sensitizers in DSSCs fabrication, and the device performance is evaluated. The better performance of the cells observed for Type-1 dyes is rationalized from electrochemical impedance spectroscopy measurements (EIS) among other techniques.

Scheme 2.1. Synthetic route adapted for the preparation of cyanoacrylic acid functionalized phenothiazine dyes for solar cell construction.

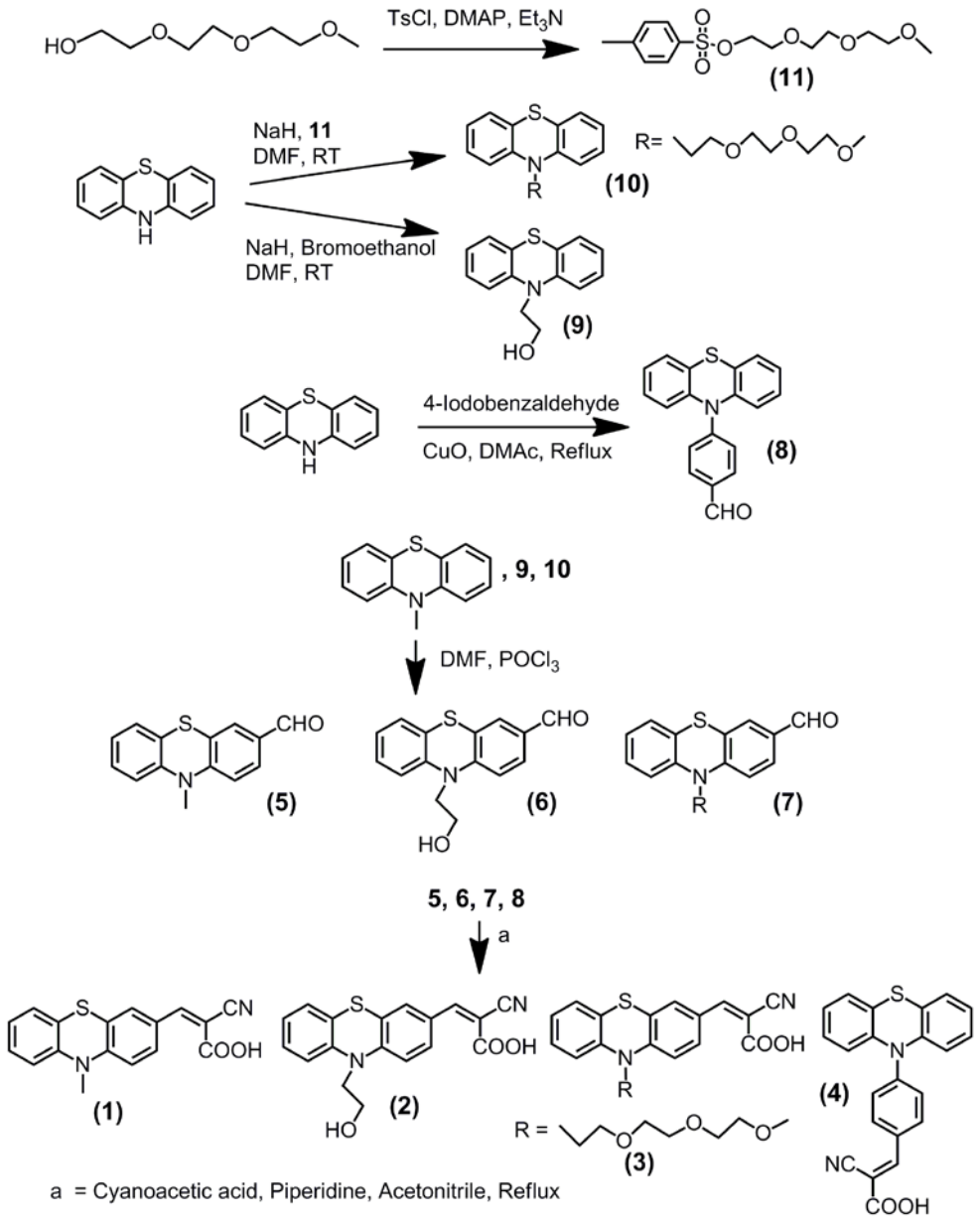

2.3. Results and Discussion

2.3.1. Syntheses of cyanoacrylic acid functionalized phenothiazine dyes. The methodology developed for the synthesis of cyanoacrylic acid functionalized at different positions of phenothiazine is shown in Scheme 2.1 while the details are given in the experimental section. Briefly, tri(ethyleneglycol)monomethylether tosylate (**11**) was synthesized by the reaction of tri(ethylene glycol)monomethyl ether with *p*-toluene sulfonyl chloride. The 10-(2-hydroxyethane)phenothiazine (**9**) was synthesized by reacting phenothiazine with 2-bromoethanol in DMF in the presence of NaH. Similarly, 10-(triethyleneglycol monomethylether) phenothiazine (**10**) was synthesized by reacting phenothiazine and **11** in DMF in the presence of NaH. Next, N-methyl phenothiazine, **10** and **11** were formylated to their respective carboxaldehyde derivatives, (**5**, **6** and **7**) by standard Vailsmeier formylation procedure by the reaction of the respective compounds with $POCl_3$ in DMF at low temperature. The 10-(4-formylphenyl) phenothiazine (**8**) was synthesized by reacting phenothiazine with 4-iodobenzaldehyde and CuO in DMAc as solvent. Finally, the electron acceptor anchoring group, cyanoacrylic acid was introduced by reacting respective phenothiazine aldehyde derivatives (**5**, **6**, **7** or **8**) with cyanoacetic acid in the presence of piperidine as catalyst in acetonitrile, to obtain compounds **1**-**4**, respectively. The newly synthesized dyes have been fully characterized by mass, ^{1}H NMR and other spectroscopic techniques.

2.3.2. Optical Absorption and Steady-State Fluorescence Studies. Figure 1a shows the absorption spectra of the investigated compounds along with pristine phenothiazine used as a control. Phenothiazine revealed a peak at 318 nm in *o*-dichlorobenzene (DCB). Introducing the cyanoacrylic acid functionality revealed drastic spectral changes. That is, for compound **4** with cyanoacrylic acid functionality at the N atom, this band was red shifted to 381 nm. Interestingly,

for compounds **1-3** having substitution at the aromatic carbon, the spectra revealed a split band, the first UV band in the 308-312 nm range and a visible band in the 420-433 nm range. Earlier, the shorter wavelength band was assigned to the localized aromatic π-π* transition of the phenothiazine ring and the long wavelength one to the charge-transfer (CT) transition.[37] The intensity of the π-π* was higher than that of the CT transition. The key observation is the spectral coverage for the two types of phenothiazine derivatives. Type-1 derivatives revealed spectral coverage from UV until about 550 nm while for the Type-2 dye, the spectral coverage was only until 450 nm. It is known that broad optical coverage is favorable for the performance of DSSCs, as more photons could be harvested.[41] Using the molar extinction coefficient of each visible band, dye concentrations were found to be 0.070 mM, 0.085 mM, 0.149 mM, and 0.041 mM, for Schemes **1**, **2**, **3**, and **4**, respectively.

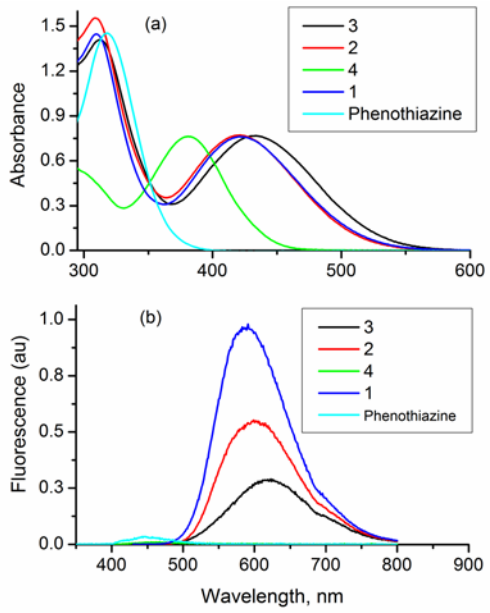

Figure 2.1. (a) Absorption (normalized to the visible band position) and (b) fluorescence emission spectrum of the indicated compounds in DCB at RT. The compounds were excited at the respective visible peak maxima.

Figure 2.1b shows the emission spectrum of the investigated compounds for concentrations normalized to the visible band intensity (Figure 2.1a) in DCB. The Type-1 phenothiazine derivatives revealed a broad emission in the range of 580-620 nm. The relative emission quantum yield was found to depend upon the type of substituent on the N-atom being **1** (methyl) > **2** (2-hydroxyethane) > **3** (triethylene glycol monomethyl ether). Interestingly, Type-2 compound, **4** and the control phenothiazine had a small emission peak around 450 nm (<2% intensity compared to Type-1 compounds). The better spectral coverage and emission properties covering most of the visible portion of the spectrum of Type-1 derivatives suggest them being better DSSC dyes compared to Type-2 dye.

2.3.3. Computational and Electrochemical Studies. Molecular orbital calculations using B3LYP/6-31G* basis set[42] were performed to arrive at the geometry and electronic structure of Type-1 and Type-2 compounds. The structures were fully optimized on Born-Oppenheimer potential energy surface, and the frequency calculations revealed absence of negative frequencies. Figure 2.2a and 2.2d show the optimized structures of **1** and **4** representing Type-1 and Type-2 compounds, respectively. The non-planar structure of phenothiazine macrocycles was clear for both types of compounds which would result in reduced dye-aggregation. That is, the angle between two terminal phenyl rings was 149^{o} from the sulfur side, and 144^{o} from the nitrogen side of the macrocycle. The cyanoacrylic acid functionality was in-plane with the substituted phenyl ring of phenothiazine in case of **1** while for **4**, the phenyl cyanoacrylic acid functionality was perpendicular the phenothiazine ring. The frontier HOMO was found to be largely located on the phenothiazine macrocycle (Figures 2.2b and e) while the LUMO was on the cyanoacrylic acid group and part of the macrocycle in case of **1** (Figure 2.2c) while for **4** it was fully on the phenyl cyanoacrylic acid functionality (Figure 2.2f). The location of the

LUMOs favors electron injection from excited phenothiazine to the semiconductor conduction band when bound to the TiO_2 surface.

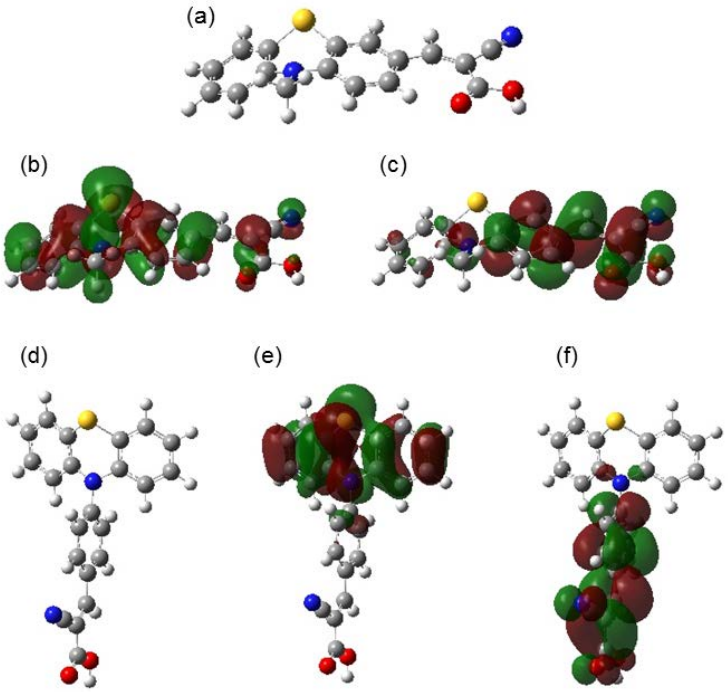

Figure 2.2. B3LYP/6-31G* optimized structures (a and d), and frontier HOMO (b and e) and LUMO (c and f) of compounds **1** (a, b and c) and **4** (d, e, f).

Further, electrochemical studies using differential pulse voltammetry were performed to evaluate the oxidation potential of the phenothiazine dyes and to estimate the energetics of electron transfer from excited dye to the conduction band of TiO_2. The first oxidation process of pristine phenothiazine was found to be located at 0.61 V vs. Fc/Fc^+ in DCB containing 0.1 M $TBAClO_4$. Substitution of cyanoacrylic acid functionality made the ring oxidation harder, more so for the Type-1 dyes compared to Type-2 dye. That is, an anodic shift of over 280 mV for Type-1 dyes (0.98 V for **2**, 0.89 V for **1** and **3** vs. Fc/Fc^+) and 110 mV for Type-2 dye (0.71 V vs. Fc/Fc^+ for **4**) was observed (see Figure 2.3). The easier oxidation of N-substituted with electron acceptor anchoring group of compound **4** was noteworthy from this study.

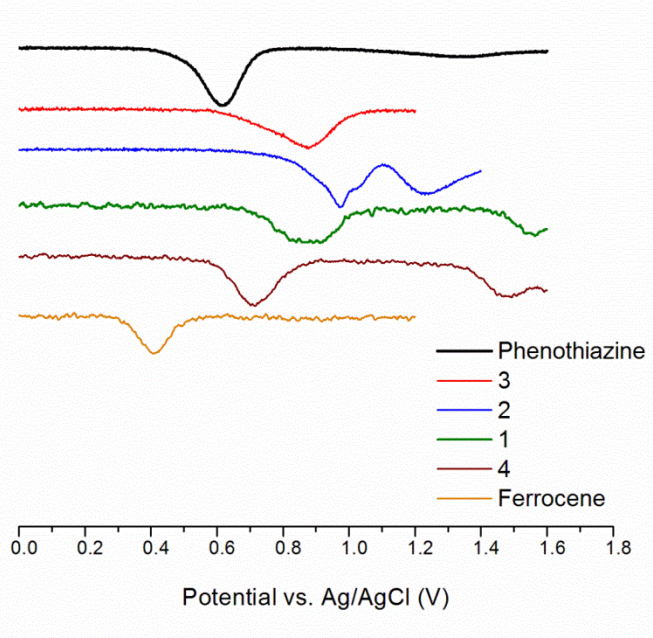

Figure 2.3. Differential pulse voltammograms of the investigated compound in acetonitrile, 0.1 M (TBA)ClO_4.

The energetics for electron injection were estimated from electrochemical and emission data. The singlet excited state energy, $E_{0\text{-}0}$ for the phenothiazine dyes were calculated from the optical absorption and emission data and were found to be 2.43-2.50 eV for Type-1 dyes and 2.97 eV for Type-2 dye. By converting the oxidation potential to SHE (1.26 V for Type-1 and 1.11 eV for Type-2 dyes) the excited state potential corresponding to the LUMO level (= $E_{ox} - E_{0\text{-}0}$) were estimated. These values were found to range between -1.17- -1.24 V for Type-1 and -1.85 V for Type-2 dyes. The sufficiently negative LUMO levels of these dyes compared to the conduction band energy of TiO_2 being -0.5 V vs. SHE implies possibility of electron injection from the excited dye into the conduction band of TiO_2. Additionally, the HOMO levels of the investigated dyes are sufficiently more positive than the iodine/iodide redox couple value being 0.40 V. This indicates the oxidized dyes formed after electron injection into the conduction bands of TiO_2 could thermodynamically accept electron from the iodide ions.

The fluorescence lifetimes of the investigated compounds were studied both in acetonitrile and modified on TiO_2 surface. Phenothiazine and the studied compounds revealed a monoexponential decay with lifetimes of 0.99, 5.02, 5.41, 5.9 and 0.55 ns, respectively, for phenothiazine, **1**, **2**, **3** and **4** (see Figure 2.4). Next, these compounds were adsorbed on quartz slide modified with thin-layer of TiO_2. Significant quenching was observed indicating occurrence of excited state events from the singlet excited phenothiazine to TiO_2. The average lifetime of compound **1** on TiO_2 surface was found to be 0.21 ns, however, for other compounds on TiO_2 surface, the lifetimes were smaller than 0.2 ns, less than the detection limit of the lifetime measurement setup used in the present study.

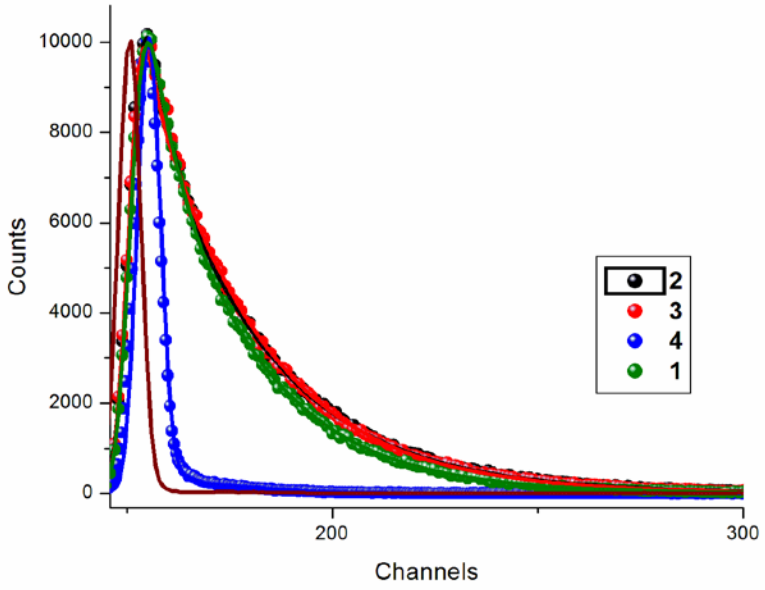

Figure 2.4. Fluorescence decay profile of the investigated compound in acetonitrile. The compounds were excited at 494 nm nano LED and the emission was collected at their respective emission band.

2.3.4. Photoelectrochemical Studies. Figure 5 shows the current-voltage characteristics of dye-sensitized solar cells employing both Type-1 and Type-2 phenothiazine dyes as sensitizers under standard global AM1.5 solar light conditions. Sandwich type two-electrode cells were built using dye-coated TiO_2 film as working electrode, platinized FTO as the counter electrode, I^-/I_3^- as redox mediator in the presence of 4-*tert*-butylpyridine in acetonitrile. The losses of light reflection and absorption by the conducting glass were not corrected. The amount of dye adsorbed was estimated by desorbing the dye using NaOH and from known molar extinction coefficient of phenothiazine. Such analysis provided ~2.2-5.0 x 10^{-7} mol/cm^2 for Type-1 and ~1.8 x10^{-7} mol/cm^2 for Type-2 dyes, being close in surface coverage of the dyes. A steady anodic photocurrent was observed when the electrodes were illuminated, and reproducible photocurrents were observed during on-off photo-switching revealing the robustness of the dye material developed here. The photovoltaic characteristic parameters of short-circuit currents density (I_{sc}), open-circuit potential (V_{oc}), fill factor (*FF*) and photovoltaic conversion efficiency preventing ethylene glycol substituent at the N-atom. On the contrary compound **4**, a Type-2 dye bearing phenyl cyanoacrylic acid functionality revealed the lowest conversion efficiency of 1.3% even though this compound was easier to oxidize by ~150 mV compared to the other studied Type-1 dyes. It is also interesting to note that although the V_{oc} were almost the same for all of the cells including that of N719 cell, the fill-factors for the phenothiazine dyes were much better than that for the N719 dye based DSSC, indicating better charge transfer kinetics.

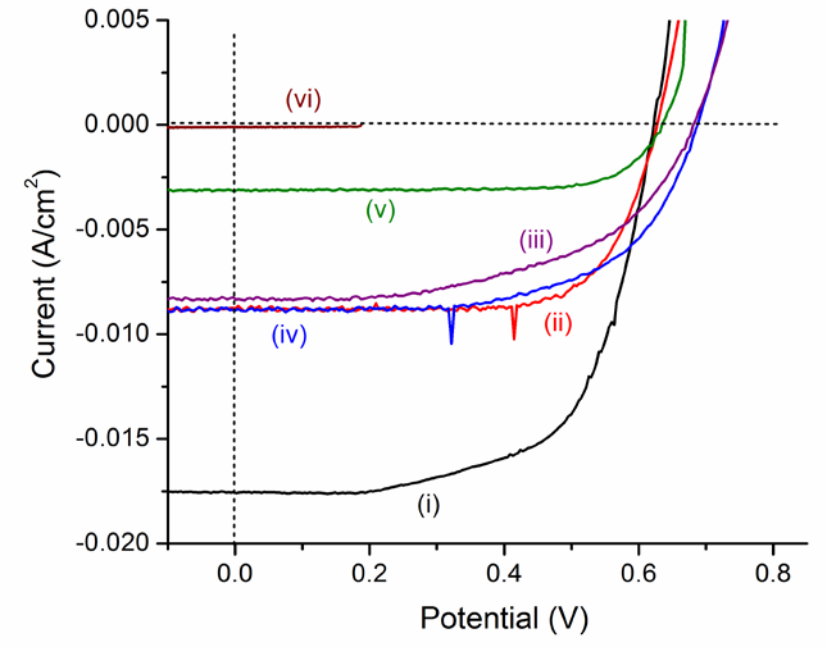

Figure 2.5. Photocurrent density vs. voltage (*I-V*) curves of DSSCs built using (i) N719, (ii) **3**, (iii) **1**, (iv) **2**, and (v) **4** dyes as sensitizers under irradiation of AM 1.5G simulated solar light (100 mW cm^{-2}) in the presence of I^-/I_3^- redox mediator in acetonitrile. The curve (vi) shows *I-V* behavior of FTO/TiO_2 in the absence of any adsorbed dye. (η) are given in Table 2.1 along with a DSSC built using N719 sensitizer for comparison. As shown in Table 2.1, photovoltaic conversion efficiencies for Type-1 dyes were higher compared to Type-2 dye. The highest □ of 4.07% was obtained for compound **3** having aggregation preventing ethylene glycol substituent at the N-atom. On the contrary compound **4**, a Type-2 dye bearing phenyl cyanoacrylic acid functionality revealed the lowest conversion efficiency of 1.3% even though this compound was easier to oxidize by ~150 mV compared to the other studied Type-1 dyes. It is also interesting to note that although the V_{oc} were almost the same for all of the cells including that of N719 cell, the fill-factors for the phenothiazine dyes were much better than that for the N719 dye based DSSC.

Table 2.1. Photovoltaic performance of DSSCs based on Type-1 and Type-2 phenothiazine dyes with liquid electrolyte.

Dye	J_{sc} (mA/cm^2)	V_{oc} (V)	*FF*	η (%)	Amount (mol/cm^2)
N719	18.13	0.62	0.66	7.39	--
1	6.50	0.66	0.75	3.21	2.18 x 10^{-7}
2	8.03	0.65	0.75	3.88	4.09 x 10^{-7}
3	8.36	0.66	0.74	4.07	5.02 x 10^{-7}
4	2.75	0.62	0.77	1.30	1.82 x 10^{-7}

The monochromatic incident photon-to-current conversion efficiency (IPCE), defined as the number of electrons generated by light in the outer circuit divided by the number of incident photons, was determined according to Equation (1)[43]

$$\text{IPCE}(\%) = 100 \times 1240 \times I_{SC}(\text{mA cm}^{-2})/[\lambda(\text{nm}) \times P_{in}(\text{mW cm}^{-2})] \qquad (1)$$

where I_{SC} is the short-circuit photocurrent generated by the incident monochromatic light and λ is the wavelength of this light with intensity P_{in}. The photocurrent action spectrum of the FTO/TiO_2 modified electrodes with listed dyes in Table 1 is shown in Figure 2.6. The Type-1 dyes efficiently converted visible light to photocurrent in the region from 400-625 nm while the Type-2 dye covered a shorter range being 400-510 nm. It is important to note that the IPCE

spectrum revealed red-shifted bands compared to absorption spectral peaks shown in Figure 1a. However, these spectral features were similar to the spectrum of the respective phenothiazine derivatives adsorbed on FTO/TiO_2 surface (see Figure 2.7). The IPCE exceeded 70% at the peak maxima, however lower in terms of spectral coverage and efficiency when compared to N719 dye based DSSC.

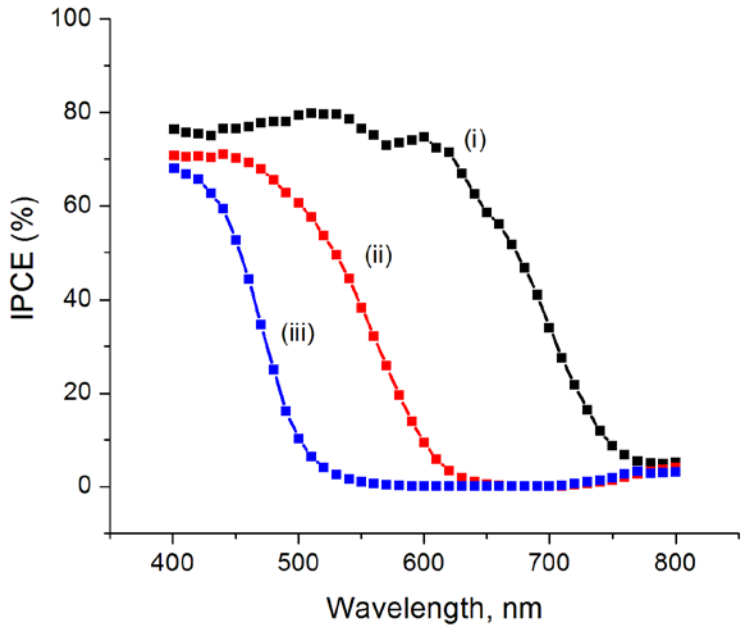

Figure 2.6. (a) Incident photon-to-current conversion action spectra of TiO_2 electrodes sensitized with (i) N719, (ii) **3** and (iii) **4** dyes in acetonitrile containing I_3^-/I^- (0.6 M PMII, 0.1 M LiI 0.05 M I_2, and 0.5 M TBP) redox mediator using an AM 1.5 simulated light source with a 350 nm UV-cut off filter.

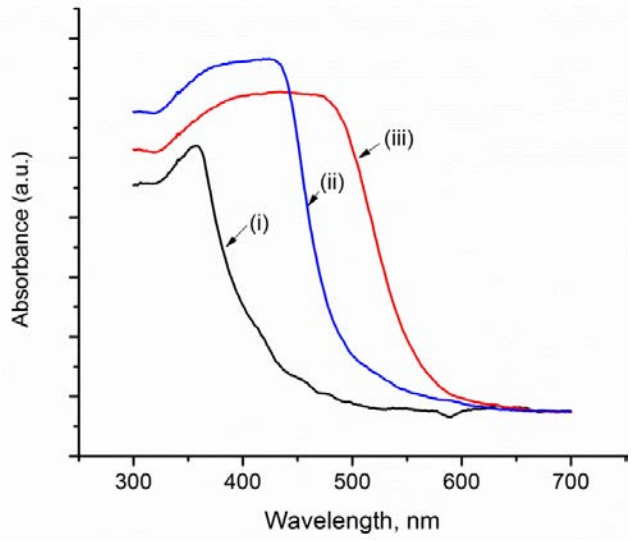

Figure 2.7. Absorption spectrum of (i) FTO covered TiO_2 film, (ii) FTO/TiO_2/**4** and (iii) FTO/TiO_2/**1**.

2.3.5. Electrochemical Impedance Spectroscopy Studies. In order to further understand the FTO/TiO_2/Dye interface, electrochemical impedance spectroscopy studies (EIS) were performed since this technique has been a useful tool to estimate electron recombination resistance and to know the dye regeneration efficiency.[43] Figure 2.8 shows EIS results for DSSCs comprised of FTO/TiO_2/**3** and FTO/TiO_2/**4** electrodes, representative of Type-1 and Type-2 type dyes, under illuminated and dark conditions covering a frequency range of 100 kHz to 50 mHz. Significant differences between Type-1 and Type-2 dye sensitized solar cells were found for the conductivity. The Nyquist plots (Figure 2.8) showed the radius of the semicircle corresponding to the working electrode to be higher for FTO/TiO_2/**4** compared to FTO/TiO_2/**3** indicating that the electron recombination resistance increases for **4** to **3** dye modified electrodes. The recombination resistance (R_{CT}) under dark conditions for FTO/TiO_2/**3** and FTO/TiO_2/**4** were 10.4 and 43.3 Ωcm^2, respectively, while these values under AM1.5 light conditions at V_{oc} were 8.0 and 36.6 Ωcm^2, respectively (see Table 2.2 for data on other Type-1 dyes). Clearly higher R_{CT} was obtained for Type-2 dyes under dark and light conditions indicating poor electron injection.

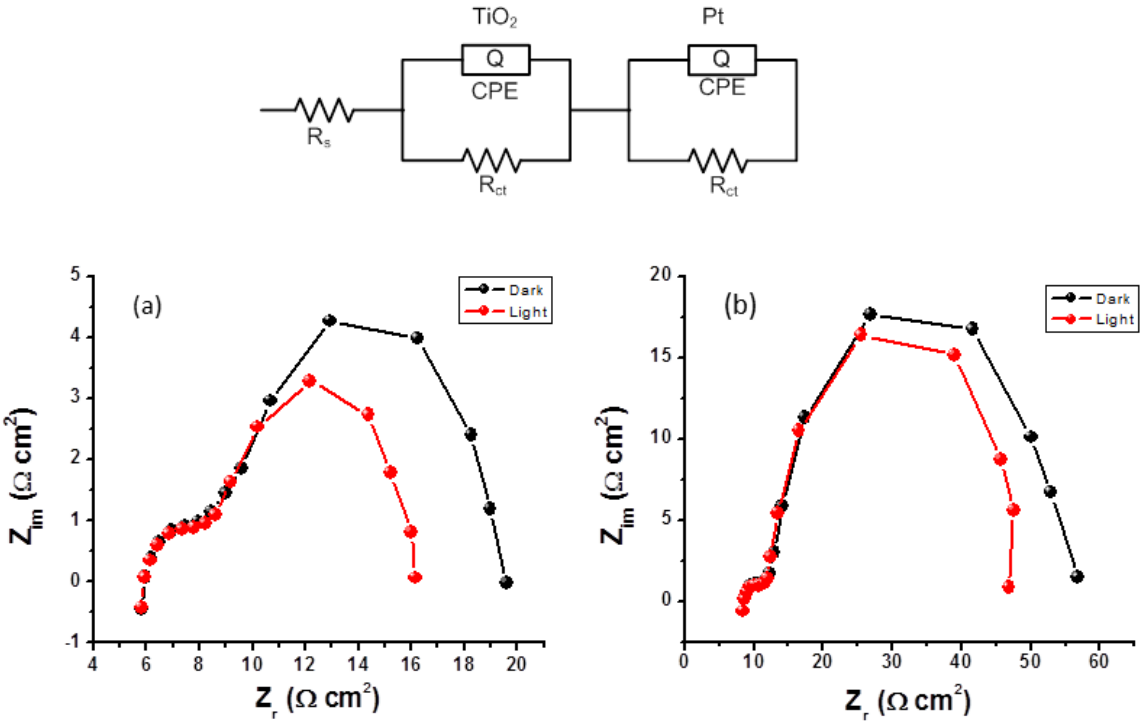

Figure 2.8. Impedance spectra (Nyquist plots) measured at the respective open circuit potential (V_{OC}) of (a) FTO/TiO_2/**3** and FTO/TiO_2/**4** in dark (dark lines) and under AM1.5 light conditions (red lines), respectively. The figure top panel shows equivalent circuit diagram used to fit the experimental data.

The decrease in recombination resistance for FTO/TiO_2/**3** compared to FTO/TiO_2/**4** under light condition can be attributed to the better performance i.e., photo-regeneration of FTO/TiO_2/**3** is much efficient in the former case, a result that agrees well with the cell efficiency shown in Figures 2.3 and 2.4. Under similar conditions N719 dye was tested and found to be in good agreement with the literature results.[42]

Table 2.2. Recombination resistance for FTO/TiO_2/Dye modified electrodes estimated from electrochemical impedance spectroscopy method.

Dye	Condition	R_{CT} Ωcm^2
1	dark	27.6
	light	17.8
2	dark	10.0
	light	6.9
3	dark	10.4
	light	8.0
4	dark	43.3
	light	36.6

2.4. Summary

In summary, four phenothiazine dyes functionalized with a cyanoacrylic acid group either directly at the macrocycle carbon (Type-1) or via macrocycle N-atom (Type-2), to unravel the structure-performance activity as solar dyes is investigated. These dyes were successfully adsorbed on noncrystalline TiO_2 particles, and efficient DSSCs have been constructed. The absorption and emission, and electrochemical properties have been extensively studied and structures were modeled using DFT calculations. It was found that the Type-1 dyes cover wider spectral range compared to Type-2 dye. Similarly, Type-1 dyes were highly fluorescent compared to Type-2 dye which was almost non-fluorescent. Electrochemical studies revealed harder oxidation potential for Type-1 dyes compared to Type-2 dyes, however, computational

LUMO was found to be located mainly on cyanoacrylic acid group for both types of dyes, needed for efficient charge injection. The emission lifetime of the adsorbed dye was found to be drastically decreased upon surface adsorption suggesting occurrence of electron transfer (charge injection) from excited phenothiazine dye to TiO_2 conduction band.

The ability of both types of phenothiazine dyes to harvest light energy into electricity was evaluated by constructing two-electrode configuration sandwich type DSSCs. Both types of dyes were capable of producing significant amounts of photocurrent and photovoltage, however, Type-1 dyes superseded the Type-2 type dye in the present DSSC assembly. The frontier orbitals generated by MO calculation revealed location of the LUMOs to be appropriate for both types of dyes for electron injection from excited dye to TiO_2 conduction band. Interestingly, the oxidation potential for Type-2 dye is smaller than that of Type-1 dyes while the excited state energy of Type-2 dye is higher than that of Type-1 dye. This implies Type-2 dye to be better in terms of energetics of charge injection, however, lower performance of the solar device was observed. Two reasons could be attributed to the poor performance of Type-2 dye, viz., poor spectral coverage and lower emission quantum yields, thus, limiting charge injection from the excited state, and higher charge recombination resistance of Type-2 dye as evaluated from electrochemical impedance spectroscopy studies. The present studies demonstrate that the simple organic dyes based on phenothiazine reported here could serve as low cost alternate to ruthenium based expensive dyes, and their performance could be fine-tuned by appropriate macrocycle functionalization. Further studies, including broadening of absorption spectra and tuning energy levels, are in progress in our laboratory.

2.5. Experimental Section

2.5.1. Chemicals. All of the reagents were from Aldrich Chemicals (Milwaukee, WI) while the bulk solvents utilized in the syntheses were from Fischer Chemicals. Tetra-*n*-butylammonium perchlorate, (TBA)ClO_4 used in electrochemical studies was from Fluka Chemicals.

2.5.2. Synthesis of phenothiazine derivatives. The general synthetic scheme and numbering of compounds is shown Scheme 1. Synthetic details are given below.

2.5.3. Tri(ethyleneglycol)monomethylether tosylate (11): - Tri(ethyleneglycol) monomethylether (3 ml, 19.14 mmol), DMAP (117 mg, 0.95 mmol) and triethyl amine (2.66 ml, 19.14 mmol) were dissolved in 100 ml of methylene chloride at 0 ^{0}C. To this mixture, 20 ml of methylene chloride solution of *p*-toluene sulfonyl chloride (3.65 g, 19.14 mmol) was added drop wise over a period of 20 min and the whole mixture was stirred for overnight at room temperature. Then the mixture was first treated with 200 ml of water and next, 200 ml of saturated solution of sodium bicarbonate. The organic compound was extracted in methylene chloride and dried over Na_2SO_4. After evaporation of the solvent, crude compound was purified by silica gel column. The desired compound was eluted with chloroform: methanol (95:5 v/v). Yield- 3.8 g (62.5%).

^{1}H NMR (400 MHz, $CDCl_3$), 2.38 ppm (s, 3H, -CH_3), 3.30 ppm (s, 3H, -CH_3), 3.45 ppm (t, 2H, -CH_2), 3.53 ppm (m,6H, -CH_2), 3.62 ppm (t, 2H, -CH_2), 4.10 ppm (t, 2H, -CH_2), 7.23 ppm (d, 2H, Ar-H), 7.70 ppm (d, 2H, Ar-H). Mass-ESI: $[M+H]^+$, obtained-319.50, calculated-318.30.

2.5.4. 10-(2-hydroxyethane)phenothiazine (9): - Compounds **8-10** were synthesized according to literature procedure with some modifications.[44-45] To an ice-cooled suspension of NaH (60% in mineral oil, 600 mg, 25 mmol) in DMF (15 ml) was added phenothiazine (2 gm, 10.05 mmol)

and 2-bromoethanol (0.71 ml, 10.05 mmol). The suspension was stirred at room temperature for five hours under N_2. The mixture was cooled at room temperature and brine was added. The organic layer was collected with methylene chloride and dried over Na_2SO_4. After evaporation of solvent, the crude compound was purified over silica gel column and desired compound was eluted using hexane: $CHCl_3$ (50:50 v/v). Yield - 1.2 g (49 %).

^{1}H NMR (400 MHz: $CDCl_3$), 3.90 ppm (t, 2H, -CH_2), 4.10 ppm (t, 2H, -CH_2), 6.85 ppm (d, 2H, Ar-H), 6.95 ppm (t, 2H, Ar-H), 7.20 ppm (m, 4H, Ar-H). Mass-ESI, $[M+H]^+$, obtained-244.50, calculated 243.60.

2.5.5. 10-Triethyleneglycol monomethylether phenothiazine (10): - To an ice-cooled suspension of NaH (60% in mineral oil, 600 mg, 25 mmol) in DMF (15 ml) was added phenothiazine (2 g, 10.05 mmol) and **11** (3.20 g, 10.05 mmol). Then, the suspension was stirred at room temperature for five hours under N_2. The mixture was cooled at room temperature and brine was added. The organic layer was collected with methylene chloride and dried over Na_2SO_4. After evaporation of solvent, the crude compound was purified over silica gel column and desired compound was eluted by hexane: $CHCl_3$ (30:70 v/v). Yield- 1.3 g (38%).

^{1}H NMR (400 MHz:$CDCl_3$), 3.35 ppm (s, 3H, -CH_3), 3.35 ppm (m, 2H, -CH_2), 3.65 ppm (m, 6H, -CH_2), 3.85 ppm (t, 2H, -CH_2), 4.10 ppm (t, 2H, -CH_2), 6.90 ppm (m, 4H, Ar-H), 7.10 ppm (m, 4H, Ar-H). Mass-ESI: $[M+H]^+$, obtained- 346.80, calculated-345.50.

2.5.6. General synthesis of phenothiazine carboxaldehyde derivatives: Compounds **1-7** were synthesized according to literature procedure with some modifications.[46-47] A solution of phenothiazine derivative (N-methylphenothiazine (**8)**, **9** or **10**) in DMF (same amount that used for preparation of Vilsmeier complex) was added to the Vilsmeier complex (formed by mixing of $POCl_3$ and DMF at 0 ^{0}C and stir for thirty minutes) and the mixture was heated overnight at 90

^{0}C under N_2. All the constituents were used in the mole ratio of 1:1:7 of phenothiazine derivatives:$POCl_3$:DMF. After cooling at room temperature mixture was kept on ice bath and treated with saturated solution of NaOH till pH of the solution was reached slightly basic (Ph 7-8); checked by litmus paper. Then the mixture was extracted by in dichloromethane and dried over sodium sulfate and evaporated to get the crude compound which was purified over silica gel column.

2.5.7. 10-Methyl-3-formyl phenothiazine (5): - Eluted by hexane: $CHCl_3$ (80:20 v/v). Yield - 53%. ^{1}H NMR (400 MHz, $CDCl_3$), 3.40 ppm (s, 3H, -CH_3), 6.80 ppm (d, 2H, Ar-H), 6.95 ppm (t, 1H, Ar-H), 7.10 ppm (d, 1H, Ar-H), 7.20 ppm (t, 1H, Ar-H), 7.55 ppm (s, 1H, Ar-H), 7.65 ppm (d, 1H, Ar-H), 9.80 ppm (s, 1H, -CHO). Mass-ESI: $[M+H]^+$, obtained-242.60, calculated-241.13.

2.5.8. 10-(2-hydroxyethane)-3-formyl phenothiazine (6**):** - Eluted by hexane: $CHCl_3$ (60:40 v/v). Yield-58.5%. ^{1}H NMR (400 MHz, $CDCl_3$). 3.80 ppm (t, 2H, -CH_2), 4.20 ppm (t, 2H, -CH_2), 6.90 ppm (m, 2H, Ar-H), 7.0 ppm (t, 1H, Ar-H), 7.15 ppm (m, 2H, Ar-H), 7.60 ppm (d, 1H, Ar-H), 7.65 ppm (d, 1H, Ar-H), 9.80 ppm (s, 1H, -CHO). Mass-ESI: $[M+H]^+$, obtained-272.40, calculated-271.13.

2.5.9. 10-Triethylene monomethylether-3-formyl phenothiazine (7): - Eluted by hexane: $CHCl_3$ (20:80 v/v). Yield- 55.7%. ^{1}H NMR (400 MHz, $CHCl_3$), 3.40 ppm (s, 3H, CH_3), 3.50 ppm (m, 2H, -CH_2), 3.70 ppm (m, 6H, -CH_2), 3.85 ppm (t, 2H, -CH_2), 4.15 ppm (t, 2H, -CH_2), 6.90 ppm (m, 2H, Ar-H), 6.95 ppm (d, 1H, Ar-H), 7.15 ppm (m, 2H, Ar-H), 7.55 ppm (s, 1H, Ar-H), 7.65 ppm (dd, 1H, Ar-H), 9.80 ppm (s, 1H, -CHO). Mass-ESI: $[M+H]^+$, obtained- 374.40, calculated-373.50.

2.5.10. 10-(4-formylphenyl) phenothiazine (8**):** - Phenothiazine (2 g, 10.05 mmol), 4-iodo benzaldehyde (2.33 g, 10.05 mmol) and CuO (3.59 g, 25.12 mmol) were kept in 100 ml RB flask under N_2 and then heated at 160 ^{0}C with DMAc as a solvent for 18 hours. After cooling at room temperature, the mixture was filtered. The filtrate was washed with water and extracted by with methylene chloride and dried over sodium sulfate. After evaporation of the solvent, the crude product was obtained which was purified over silica gel column. The desired compound was eluted by hexane:$CHCl_3$ (50:50 v/v). Yield- 1.5 g (49 %). ^{1}H NMR (400 MHz, $CDCl_3$), 7.0 – 7.10 ppm (m, 4H, Ar-H), 7.15 – 7.25 ppm (m, 4H, Ar-H), 7.35 ppm (d, 2H, Ar-H), 7.65 ppm (d, 2H, Ar-H), 9.75 ppm (s, 1H, Ar-H). Mass-ESI: $[M+H]^+$, obtained-305.30, calculated-304.20.

2.5.11. Preparation of phenothiazine cyanoacrylic acid derivatives: - Phenothiazine aldehyde derivatives and cyanoacetic acid (1:2 mole ratio) were mixed and refluxed in the presence of piperidine (catalytic amount) in acetonitrile (15 ml) as a solvent under N_2 for five hours. After removing the solvent, mixture was washed with water and extracted by with methylene chloride and dried over Na_2SO_4. After evaporation, the crude compound was obtained which was purified by silica column. The desired compounds were eluted by $CHCl_3$:MeOH (90:10 v/v).

2.5.12. 10-Methyl-3-cyanoacrylic acid phenothiazine (1): - Yield-45%. ^{1}H NMR (400 MHz, $CDCl_3$). 3.40 ppm (s, 3H, -CH_3), 6.80 ppm (m, 2H, Ar-H), 6.95 ppm (t, 1H, Ar-H), 7.10 ppm (d, 1H, Ar-H), 7.20 ppm (t, 1H, Ar-H), 7.65 ppm (s, 1H, Ar-H), 7.80 ppm (d, 1H, Ar-H), 7.95 ppm (s, 1H, alkene-H). Mass-ESI: $[M]^+$, calculated 308.35, found 263.1, 277.1 (84%), 307.0 (80%) (100%). Elemental analysis: calculated for $C_{17}H_{12}N_2O_2S$: C:66.21%, H:3.92%, N:9.08%, found: C:67.25%, H:4.69%, N:10.01%.

2.5.13. 10-(2-hydroxy ethane)-3-cyanoacrylic acid phenothiazine (2): - Yield-38%. ^{1}H NMR (400 MHz, $CDCl_3$), 3.60 ppm (t, 2H, -CH_2), 4.10 ppm (t, 2H, -CH_2), 6.65 ppm (d, 1H, Ar-H),

6.73 ppm (d, 1H, Ar-H), 6.93 ppm (t, 1H, Ar-H), 7.05 ppm (d, 1H, Ar-H), 7.15 ppm (t, 1H, Ar-H), 7.50 ppm (s, 1H, Ar-H), 7.70 ppm (d, 1H, Ar-H), 8.0 ppm (s, 1H, Alkene-H). Mass-ESI: $[M]^+$, calculated 338.38, found 326.2 (100%), 341.2 (10%). Elemental analysis: calculated for $C_{18}H_{14}N_2O_3S$: C:63.89%, H:4.17%, N:8.28%, found: C:62.21%, H:4.65%, N:7.81%. FT-IR in KBr pallet (major peaks): 3412, 2949, 2213, 1620, 1593, 1571, 1468, 1360, 1334, 1221, 816, 751, 616 cm^{-1}.

2.5.14. 10-Triethyleneglycol monomethylether-3-cyanoacrylic acid phenothiazine (3): - Yield- 30%. ^1H NMR (400 MHz, $CDCl_3$), 3.40 ppm (s, 3H, $-CH_3$), 3.60 ppm (t, 2H, $-CH_2$), 3.70 ppm (m, 6H, $-CH_2$), 3.90 ppm (t, 2H, $-CH_2$), 4.20 ppm (t,2H, $-CH_2$), 6.65 ppm (d, 1H, Ar-H), 6.77 ppm (d, 1H, Ar-H), 6.93 ppm (t, 1H, Ar-H), 7.08 ppm (d, 1H, Ar-H), 7.15 ppm (t, 1H, Ar-H), 7.52 ppm (s, 1H, Ar-H), 7.65 ppm (d, 1H, Ar-H), 8.0 ppm (s, 1H, alkene-H). Mass-ESI: $[M]^+$, calculated 440.50, found 395.1 (100%), 439.1 (82%), . Elemental analysis: calculated for $C_{23}H_{24}N_2O_5S$: C:62.71%, H:5.41%, N:6.36%, found: C:60.57%, H:5.74%, N:6.82%. FT-IR in KBr pallet (major peaks): 3469, 2945, 3414, 2212, 1636, 1618, 1357, 1113, 812, 750, 617 cm^{-1}.

2.5.15. 10-(4-cyanoacrylic acid phenyl)phenothiazine (4): - Yield- 30%. ^1H NMR (400 MHz, $CDCl_3$), 6.92 ppm (dd, 2H, Ar-H), 7.0 ppm (m, 2H, Ar-H), 7.10 ppm (m, 4H, Ar-H), 7.2 ppm (dd, 2H, Ar-H), 7.84 ppm (d, 2H, Ar-H), 8.0 ppm (s, 1H, alkene-H). Mass-ESI: $[M]^+$, calculated 370.40, found 325.1 (94%), 339.1 (92%) and 369.1 (100%). Elemental analysis: calculated for $C_{22}H_{14}N_2O_2S$: C:71.33%, H:3.81%, N:7.56%, found: C:69.45%, H:5.09%, N:8.62%.

2.5.16. TiO_2 electrode preparation. FTO glass electrodes were first washed with soap and water, followed by sonication for ten minutes in each of the following solutions: 0.1 M HCl in ethanol, bulk acetone, and bulk isopropanol. Following a drying period, the electrodes were then submerged in a 40 mM solution of $TiCl_4$ in MilliQ water for thirty min at 75° C. The electrodes

were then washed with MilliQ water, then MeOH before applying tape to each side, to control the film thickness and provide space between the film and the edge of the FTO. Before applying the TiO_2 paste, each electrode was dusted thoroughly with nitrogen gas. The first layer applied used a paste derived from 20 nm TiO_2 particles (PST-18NR) using Doctor-blade technique and allowed to dry in air for twenty min. This was followed by a heating cycle at temperatures of 130° C, 230° C, 330° C, 395° C, 430° C, and 515° C, for ten min each. After allowing the electrode to cool at 80° C, a second layer of 20 nm TiO_2 paste was then applied, followed by the same heating cycle. Lastly, a layer of 400 nm TiO_2 paste (PST-400C) was applied, followed by the heating cycle. After cooling, each piece of FTO was cut into 5-6 smaller electrodes of similar size. The electrodes were then submerged in a fresh 40 mM $TiCl_4$ solution for another thirty minutes at 75° C. Afterwards, each electrode was submerged in a 0.3 mM dye solution in DCM overnight with the TiO_2 film facing up.

2.5.17. Platinized electrode preparation. FTO glass electrodes were washed as stated above. After washing, each strip of FTO was heated at 440° C for fifteen minutes, and then cooled at 80° C for another ten minutes. Each strip of FTO was then cut into 5-6 smaller electrodes of similar size. Each electrode was then dusted with N_2 before applying a solution containing 1 mg of chloroplatinic acid in 2 mL of EtOH. The electrodes were heated at 440° C a second time, before allowing to cool.

2.5.18. Spectral Measurements. The UV-visible spectral measurements were carried out either on a Shimadzu Model 2550 double monochromator UV-visible spectrophotometer or a Jasco V-670 spectrophotometer. The steady-state fluorescence spectra were measured by using a Horiba Jobin Yvon Nanolog UV-visible-NIR spectrofluorometer equipped with a PMT (for UV-visible) and InGaAs (for NIR) detectors. The lifetimes were measured with the Time Correlated Single

Photon Counting (TCSPC) lifetime option with nano-LED excitation sources on the Nanolog. The time calibration factor for system was 0.439 ns per channel. All the solutions were purged using nitrogen gas prior to spectral measurements. A right angle detection method was used for emission measurements. The ^{1}H NMR studies were carried out on a Bruker 400 MHz spectrometer. Tetramethylsilane (TMS) was used as an internal standard. Differential pulse voltammograms were recorded on an EG&G 263A potentiostat/galvanostat using a three electrode system. A platinum button electrode was used as the working electrode. A platinum wire served as the counter electrode and an Ag/AgCl electrode was used as the reference electrode. Ferrocene/ferrocenium redox couple was used as an internal standard. All the solutions were purged prior to electrochemical and spectral measurements using argon gas. The computational calculations were performed by DFT B3LYP/6-31G* methods with GAUSSIAN 09 software package[42] on high speed computers. The HOMO and LUMO orbitals were generated using *GuessView* program.

2.5.19. Photoelectrochemical and Electrochemical Impedance Measurements. Photoelectrochemical experiments were performed in a two-electrode configuration; thin films of TiO_2 on FTO was developed using Doctorblade technique according literature procedure.[4] Photoelectrochemical cells were constructed using platinized ITO as counter electrode in acetonitrie containing a 0.5 M (n-Bu_4)NI and 0.03 M I_2 as redox mediator. The photocurrent-photovoltage characteristics of the solar cells were measured using a Model 2400 Current/Voltage Source Meter of Keithley Instruments, Inc. (Cleveland, OH) under illumination with an AM 1.5 simulated light source using a Model 9600 of 150-W Solar Simulator of Newport Corp. (Irvine, CA). Incident photon-to-current efficiency (IPCE) measurements were performed under ~4 mW cm^{-2} monochromatic light illumination conditions using a setup

comprised of a 150 W Xe lamp with a Cornerstone 260 monochromator (Newport Corp., Irvine, CA).

Electrochemical impedance measurements were performed using EG&G PARSTAT 2273 potentiostat. Impedance data were recorded under forward bias condition from 100 kHz to 50 mHz with an A.C amplitude of 10 mV. Data were recorded under dark and A.M 1.5 illumination conditions applying corresponding open circuit potential (V_{oc}) for each electrode. The data were analyzed using ZSimpwin software from Princeton Applied Research. Solution resistance (R_s), charge transfer resistance (R_{ct}), and capacitance due to constant phase element (Q) was deduced from the fitted data. CPE was considered as capacitance component of the double layer electrode interface due to roughness of the electrode.

2.6. References

1. O'Regan B.; Grätzel, M. *Nature,* **1991**, *353*, 737.

2. Chen, S.; Xu, X.; Liu, Y.; Yu, G.; Sun, X.; Qiu, W.; Ma, Y.; Zhu, D. *Adv. Funct. Mater.*, **2005**, *15*, 1541.

3. Yoon, K. R.; Ko, S.-O.; Lee, S. M.; Lee, H. *Dyes Pigm.*, **2007**, *75*, 567.

4. Lai, R. Y.; Fabrizio, E. F. Lu, L.; Jenekhe, S. A.; Bard, A. J. *J. Am. Chem. Soc.*, **2001**, *123*, 9112.

5. Tsai, Y.-L.; Chang, C.-C.; Kang, C.-C.; Chang, T.-C. *J. Lumin.*, **2007**, *127*, 41.

6. Roquet, S.; Cravino, A.; Leriche, P.; Alévêque, O.; Frère, P.; Roncali, J. *J. Am. Chem. Soc.*, **2006**, *128*, 3459.

7. Mishra, A.; Fischer, M. K. R.; Bäuerle, P. *Angew. Chem., Int. Ed.*, **2009**, *48*, 2474.

8. Hara, K.; Kurashige, M.; Ito, S.; Shinpo, A.; Suga, S.; Sayama, K.; Arakawa, H. *Chem. Commun.*, **2003**, 252.

9. Kitamura, T.; Ikeda, M.; Shigaki, K.; Inoue, T.; Anderson, N. A.; Ai, X.; Lian, T.; Yanagida, S. *Chem. Mater.*, **2004**, *16*, 1806.

10. Hara, K.; Sato, T.; Katoh, R.; Furube, A.; Yoshihara, T.; Murai, M.; Kurashige, M.; Ito, S.; Suga, S.; Arakawa, H. *Adv. Funct. Mater.*, **2005**, *15*, 246.

11. Wang, Z. S.; Cui, Y.; Dan-oh, Y.; Kasada, C.; Shinpo, A.; Hara, K.; *J. Phys. Chem. C*, **2007**, *111*, 7224.

12. Xu, W.; Peng, B.; Chen, J.; Liang, M.; Cai, F. *J. Phys. Chem. C*, **2008**, *112*, 874.

13. Liu, W.-H.; Wu, I. C.; Lai, C.-H.; Lai, C.-H.; Chou, P.-T.; Li, Y.-T.; Chen, C.-L.; Hsu, Y.-Y. Chi, Y. *Chem. Commun.*, **2008**, 5152.

14. Hwang, S.; Lee, J. H.; Park, C.; Lee, H.; Kim, C.; Park, C.; Lee, M.-H.; Lee, W.; Park, J.; Kim, K.; Park, N.-G.; Kim, C. *Chem. Commun.*, **2007**, 4887.

15. Ito, S.; Zakeeruddin, S. M.; Humphry-Baker, R.; Liska, P.; Charvet, R.; Comte, P.; Nazeeruddin, M. K.; Péchy, P.; Takata, M.; Miura, H.; Uchida, S.; Grätzel, M. *Adv. Mater.*, **2006**, *18*, 1202.

16. Ito, S.; Miura, H.; Uchida, S.; Takata, M.; Sumioka, K.; Liska, P.; Comte, P.; Péchy, P.; Grätzel, M. *Chem. Commun.*, **2008**, 5194.

17. Tian, H.; Yang, X.; Chen, R.; Pan, Y.; Li, L.; Hagfeldt, A.; Sun, L. *Chem. Commun.*, **2007**, 3741.

18. Cao, D.; Peng, J.; Hong, Y.; Fang, X.; Wang, L.; Meier, H. *Org. Lett.*, 2011, **13**, 1610 .

19. Xie, Z.; Midya, A.; Loh, K. P.; Adams, S.; Blackwood, D. J.; Wang, J.; Zhang, X.; Chen, Z. *Prog. Photovoltaics*, **2010**, *18*, 573.

20. Wu, W.; Yang, J.; Hua, J.; Tang, J.; Zhang, L.; Long, Y.; Tian, H. *J. Mater. Chem.*, **2010**, *20*, 1772.

21. Smestad, G. P.; Spiekermann, S.; Kowalik, J.; Grant, C. D.; Schwartzberg, A. D.; Adam, M.; Zhang, J.; Tolbert, L. M.; Moons, E. *Solar Energy Mater. & Solar Cells*, **2003**, *76*, 85-105.

22. Wu, S-L.; Lu, H.-P.; Yu, H.-T.; Chuang, S.-H.; Chiu, C.-L.; Lee, C. W.; Diau, E. W.-G.; Yeh, C.-Y. *Energy and Environ. Sci*. **2010**, *3*, 949.

23. (a) Lee, C. Y.; Hupp. J. T. *Langmuir*, **2010**, *26*, 3760. (b) Walter, M. G.; Rudine, A. B.; Wasmer, C. C. *J. Porphyrins Phthalocyanines*, **2010**, *14*, 759.

24. Kamat, P. V. *J. Phys. Chem. C*, **2007**, *111*, 2834.

25. (a) Umeyama T.; Imahori, H. *Energy Environ. Sci.*, **2008**, *1*, 120. (b) Imahori, H.; Umeyama, T.; Kurotobi, K.; Takano, Y. *Chem. Commun*. **2012**, *48*, 4032.

26. Hasobe, T. *Phys. Chem. Chem. Phys.*, **2010**, *12*, 44.

27. Subbaiyan, N. K.; Wijesinghe, C. A.; D'Souza, F. *J. Am. Chem. Soc*., **2009**, *131*, 14646.

28. Parussulo, A. L. A.; Iglesias, B. A.; Toma, H. E.; Araki, K. *Chem. Commun*. **2012**, *48*, 6939.

29. (a) Ragoussi, M.-E.; Cid, J.-J. Yum, J.-H.; de la Torre, G.; Di Censo, D.; Gratzel, M.; Nazeeruddin, M. E.; Torres, T. *Angew. Chem. Int. Ed. Engl*. **2012**, *51*, 4375. (b) Martinez-Diaz, M. V.; de la Torre, G.; Torres, T. *Chem. Commun*. **2010**, *46*, 7090.

30. Sargent, E. H.; *Nature Photonics*, **2012**, *6*, 133.

31. Bang, J. H.; Kamat, P. V. *ACS Nano*, **2009**, *3*, 1467.

32. Tang, J.; Wang, X.; Brzozowski, L.; Barkhouse, D.; Aaron, R.; Debnath, R.; Levina, L.; Sargent, E. H. *Adv. Mater*. **2010**, *22*, 1398.

33. D'Souza, F.; Ito, O. *Chem. Soc. Rev*. **2012**, *41*, 86.

34. D'Souza, F.; Sandanayaka, A. S. D.; Ito, O. *J. Phys. Chem. Letts.* **2010**, *1*, 2586.

35. Kamat P. V.; Schatz, G. C. *J. Phys. Chem. C*, **2009**, *113*, 15473.

36. Rochford, J.; Chu, D.; Hagfeldt, A.; Galoppini, E. *J. Am. Chem. Soc.* **2007**, *129*, 4655.

37. Wu, W.; Yang, J.; Hua, J.; Tang, J.; Zhang, L.; Long, Y.; Tian, H. *J. Mater. Chem*. **2010**, *20*, 1772.

38. Wan, Z.; Jia, C.; Duan, Y.; Zhang, J.; Lin, Y.; Shi, Y. *Dye & Pigments*, **2012**, *94*, 150.

39. Xie, Z.; Midya, A.; Loh, K. P.; Adams, S.; Blackwood, D. J.; Wang, J.; Zhang, X.; Chen, Z. *Prog. Photovolt.: Res. Appl*. **2010**, *18*, 573.

40. Marszalek, M.; Nagane, S.; Ichake, A.; Hamphry-Baker, R.; Paul, V.; Zakeeruddin, S. M.; Gratzel, M. *J. Mater. Chem*. **2012**, *22*, 889.

41. Hara, K.; Mori, S. S. *Handbook of Photovoltaic Science and Engineering*, Ed. Luque, A.; Hegedus, John-wley, Chichester, UK, 2011, 642.

42. *Gaussian 09*, Frisch, M. J.; Trucks, G. W.; Schlegel, H. B.; Scuseria, G. E.; Robb, M. A.; Cheeseman, J. R.; Zakrzewski, V. G.; Montgomery, J. A.; Stratmann, R. E.; Burant, J. C.; Dapprich, S.; Millam, J. M.; Daniels, A. D.; Kudin, K. N.; Strain, M. C.; Farkas, O.; Tomasi, J.; Barone, V.; Cossi, M.; Cammi, R.; Mennucci, B.; Pomelli, C.; Adamo, C.; Clifford, S.; Ochterski, J.; Petersson, G. A.; Ayala, P. Y.; Cui, Q.; Morokuma, K.; Malick, D. K.; Rabuck, A. D.; Raghavachari, K.; Foresman, J. B.; Cioslowski, J.; Ortiz, J. V.; Stefanov, B. B.; Liu, G.; Liashenko, A.; Piskorz, P.; Komaromi, I.; Gomperts, R.; Martin, R. L.; Fox, D. J.; Keith, T.; Al-Laham, M. A.; Peng, C. Y.; Nanayakkara, A.; Gonzalez, C.; Challacombe, M.; Gill, P. M. W.; Johnson, B. G.; Chen, W.; Wong, M. W.; Andres, J. L.; Head-Gordon, M.; Replogle, E. S.; Pople, J. A. Gaussian, Inc., Pittsburgh PA, 2009.

43. *Dye-Sensitized Solar Cells*, Ed. Kalyanasundaram, EPFL Press, Lausanne, 2010.

44. Xu, T.; Lu, R.; Liu, X.; Zheng, X.; Qui, X.; Zhao, Y. *Org. Letts*. **2007**, *9*, 797.

45. Xu, T.; LU, R.; Liu, X.; Chen, P.; Qui, X.; Zhao, Y. *Eur. J. Org. Chem*. **2008**, 1065.

46. Tian, H.; Yang, X.; Chen, R.; Pan, Y.; Li, L.; Hagfeldt, A.; Sun, L.; *Chem. Commun*. **2007**, 3741.

47. Gaina, L.; Porumb, D.; Silaghi-Dumitrescu, I.; Cristea, C.; Silaghi-Dumitrescu, L.; *Can. J. Chem*. **2010**, *88*, 42.

CHAPTER 3

PORPHYRIN-SENSITIZED SOLAR CELLS: EFFECT OF CARBOXYL ANCHOR GROUP ORIENTATION ON THE CELL PERFORMANCE[†]

3.1. Abstract

The effect of the orientation of the porphyrin sensitizer onto the TiO_2 surface on the performance of dye sensitized solar cells (DSSCs) is reported. Free-base and zinc porphyrins bearing a carboxyl anchoring group at the *para*, *meta*, or *ortho* positions of one of the *meso*-phenyl rings were synthesized for application in Grätzel-type photoelectrochemical cells. The remainder of the *meso*-phenyl rings was substituted with alkyl chains of different length to visualize any aggregation effects. Absorption and fluorescence studies were performed to characterize and observe spectral coverage of the thirteen newly synthesized porphyrin derivatives. Photoelectrochemical studies were performed after immobilization of porphyrins onto nanocrystalline TiO_2 and compared with DSSC constructed using N719 dye as reference. The performance of DSSCs with the porphyrin anchoring at the *para* or *meta* position were found to greatly exceed those with the anchoring group in the *ortho* position. Additionally, cells constructed using zinc porphyrin derivatives outperformed the free-base porphyrin analogs. Better dye regeneration efficiency for the zinc porphyrin derivatives compared to their free-base porphyrin analogs, and for the *meta* and *para* derivatives over the *ortho* derivatives was evaluated from electrochemical impedance spectroscopy studies. Femtosecond transient

[†] Reproduced in full with permission from Hart, A.S.; KC, C.B.; Gobeze, H.B.; Sequeira, L.R.; D'Souza, F. *ACS Appl. Mater. Interfaces.* **2013**, 5, 5314. Copyright 2013 American Chemical Society.

absorption spectroscopy studies were performed to probe the kinetics of charge injection and charge recombination with respect to the orientation of porphyrin macrocycle on TiO_2 surface. The *ortho* porphyrin derivative with an almost flat orientation to the TiO_2 surface revealed fast charge recombination and suggested occurrence of through-space charge transfer. The overall structure-performance trends observed for the present porphyrin DSSCs have been rationalized based on spectral, electrochemical, electrochemical impedance spectroscopy and transient spectroscopy results.

3.2. Introduction

Dye-sensitized solar cells (DSSCs), often known as Grätzel cells, have garnered significant attention as promising low-cost alternatives to expensive Si-based solar cell technology.[1-12] In typical DSSCs, mesoporous titanium dioxide (TiO_2) decorated with photosensitizer dye molecules inject electrons into the conduction band of TiO_2 in contact with an electrolyte solution, achieving light into electricity conversion.[13-41] Organic photosensitizers capable of wide spectral capture are considered to be cheaper alternatives for DSSC applications, potentially replacing the originally designed, rather expensive ruthenium-based metal complex sensitizers. Additionally, organic dyes possess higher extinction coefficients, leading to greater light harvesting abilities. Common solar dye design involves an electron donor photosensitizer connected to an electron acceptor that doubles as an anchoring functional group. Coumarins, quantum dots, triphenylamines, phenothiazine, phthalocyanine, and porphyrin are commonly implemented as photosensitizers.[42-108]

Among the different organic dyes, functionalized porphyrins are frequently used sensitizers.[84-108] These tetrapyrrole macrocycles, in their free-base form or with a redox inactive

metal such as zinc inside the macrocycle cavity, reveal strong light absorption with a Soret band in the 400-450 nm range and visible bands in the 500-650 nm range. In fact, the highest efficiency solar cell reported to-date (η = 12.3%) is of a zinc porphyrin based dye molecule.[108] One key issue to consider in designing porphyrin dyes relates to the position of the anchoring group in relation to the plane of macrocycle π-system. In a majority of the porphyrin derived dyes, the carboxyl anchoring group was positioned in such a way that the porphyrin was orthogonal to the TiO_2 surface, although few studies have shown that the positioning of carboxyl group vary the performance of the solar cells.[100-104]

In the present study, thirteen porphyrin derivatives, six free-base and seven zinc-metallated, are investigated by varying the position of the carboxyl anchoring group: *para* (**1p**, **1p-Zn**, **2p, 2p-Zn, 3p-Zn**), *meta* (**1m**, **1m-Zn**, **3m, 3m-Zn, 2m, 2m-Zn)**, and *ortho* (**1o** and **1o-Zn**), and length of the alkyl substituents on the remaining three phenyl rings for their cell performance (see Figure 3.1 for structures). As shown in Figure 3.2, as a result of fairly rigid bidentate type binding of the carboxyl group on TiO_2,[100-104] the *para* derivatives would largely position the porphyrin π-system orthogonal to the TiO_2 surface; *meta* derivatives would position the π-system at an angle (50-80^o) which could favor both through-bond and through-space interactions; and the *ortho* derivatives would bring the π-system even closer to the TiO_2 surface facilitating stronger through-space interactions between them. Thus a minor modification of carboxyl functionality would change the relative orientation of the porphyrin with respect to TiO_2 surface, and would contribute to the overall cell performance. We report these findings from a systematic study performed using different techniques.

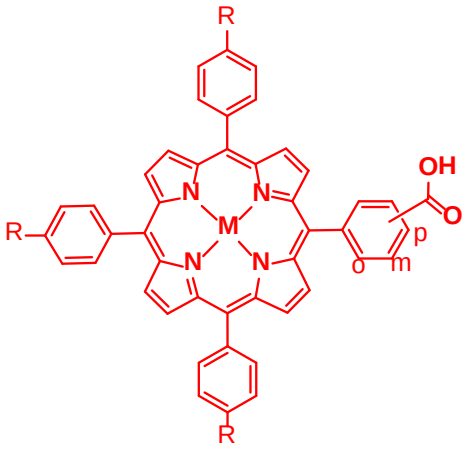

R = -CH_3; M = 2H; para **1p**
R = -CH_3; M = 2H; meta **1m**
R = -CH_3; M = 2H; ortho **1o**
R = -CH_3; M = Zn; para **1p-Zn**
R = -CH_3; M = Zn; meta **1m-Zn**
R = -CH_3; M = Zn; ortho **1o-Zn**
R = -$(OCH_2CH_2)_3OCH_3$; M = 2H, para **2p**
R = -$(OCH_2CH_2)_3OCH_3$; M = 2H, meta **2m**
R = -$(OCH_2CH_2)_3OCH_3$; M = Zn, para **2p-Zn**
R = -$(OCH_2CH_2)_3OCH_3$; M = Zn, meta **2m-Zn**
R = -$CH_2CH_2CH_3$; M = 2H, meta **3m**
R = -$CH_2CH_2CH_3$; M = Zn, para **3p-Zn**
R = -$CH_2CH_2CH_3$; M = Zn, meta **3m-Zn**

Figure 3.1. Structures of the synthesized porphyrin derivatives with the anchoring carboxyl group located either at the *para*, *meta* or *ortho* position of one of the phenyl rings.

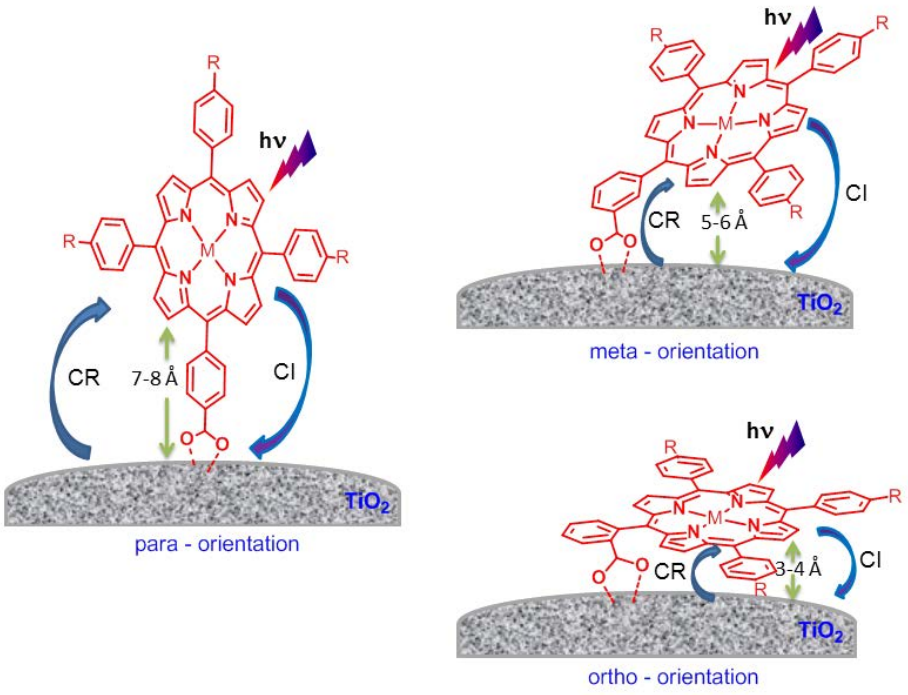

Figure 3.2. Relative orientation of *para*, *meta* and *ortho* carboxyphenyl functionalized porphyrin adsorbed on TiO_2 surface. Key photochemical events responsible for cell performance are also shown (CI - charge injection; CR - charge recombination).

3.3. Results

The syntheses of the free-base porphyrin derivatives was carried out according to the traditional Adler-Longo method by reacting stoichiometric amounts of pyrrole and functionalized benzaldehydes in propionic acid followed by chromatographic separation over silica gel.[109] The free-base porphyrins were metallated using zinc acetate in refluxing chloroform/methanol solution while monitoring the completeness of the reaction by recording the disappearance of the 515 nm band of the free-base porphyrin.[110] The purity of all the porphyrin derivatives was checked on thin-layer chromatography prior to performing any studies.

3.3.1. Optical Absorbance and Steady-State Fluorescence Studies. The optical absorption and emission spectra of the carboxyl functionalized porphyrins in chloroform/methanol mixture were not significantly different from their parent derivatives, *viz*., tetrakis(4-alkylphenyl)porphyrins.[111-112] Representative absorption and emission spectrum of **1p-Zn** is shown in Figure 3. The free-base porphyrins exhibited a strong Soret in the 420 nm range and four visible bands in the 500-675 nm range while for zinc porphyrins the Soret was red-shifted by about 5 nm compared to the respective free-base porphyrin analog and two visible bands in the 525-575 nm range, due to increased symmetry, were observed. The fluorescence spectra of the free-base porphyrins revealed strong emission around 650 with a shoulder band at 720 nm, while for the zinc porphyrins, these emission bands were at 615 and 665 nm, respectively.

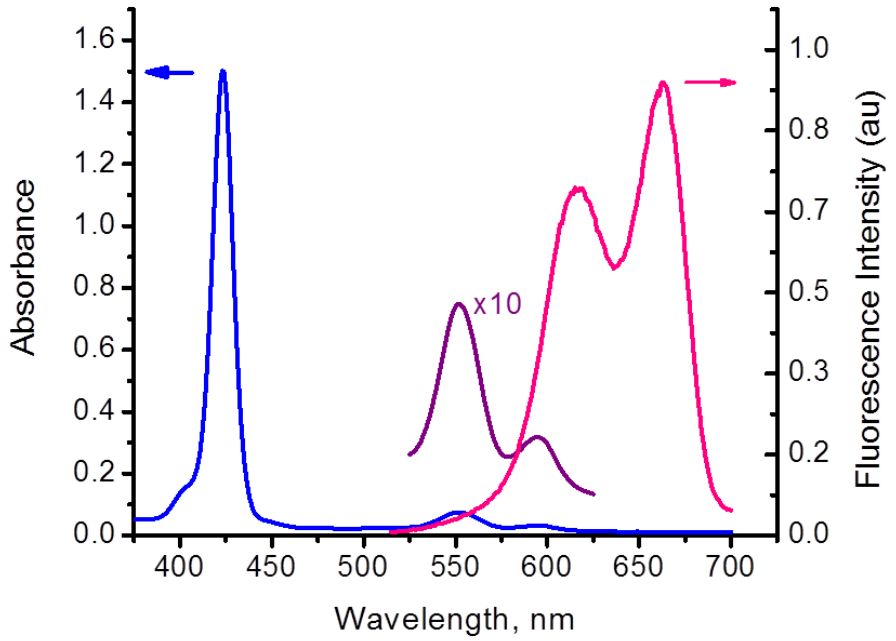

Figure 3.3. Absorption and fluorescence spectrum of **1p-Zn** in chloroform-methanol mixture. The Q-band region is magnified for clarity.

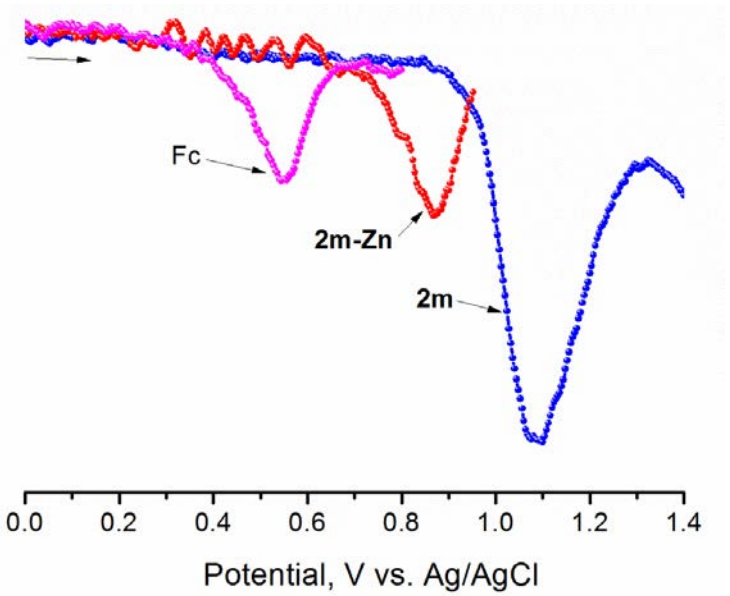

Figure 3.4. Differential pulse voltammograms showing first oxidations of **2m**, **2m-Zn** and ferrocene (used as internal standard) in DMF containing 0.1 M $(TBA)ClO_4$.

The expected two one-electron oxidation and two one-electron reduction for each of the porphyrin derivatives were also observed.[113] The zinc porphyrin derivatives were easier to oxidize by about 220 mV compared to their free-base porphyrin analogs (Figure 3.4). Further, to visualize the spectral features of the oxidized electron donor sensitizer porphyrin, compounds **1p-Zn**, **1m-Zn**, and **1o-Zn** were chemically oxidized by the addition of one equivalent of nitrosonium tetrafluoroborate in methanol. Figure 3.5 shows spectral changes for **1p-Zn** while for **1m-Zn** and **1o-Zn** the spectral are shown in Figure 3.6. New bands with peak maxima at 660 nm and at 845 nm were apparent for the $ZnP^{\cdot+}$ species.

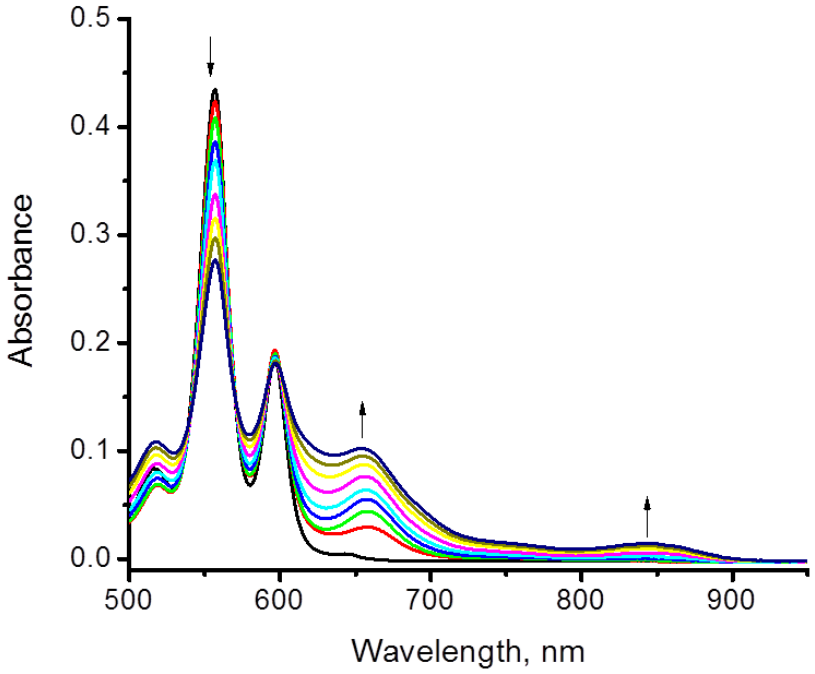

Figure 3.5. Chemical oxidation of porphyrin **1p-Zn** using nitrosonium tetrafluoroborate (0.15 eq. each addition) in methanol.

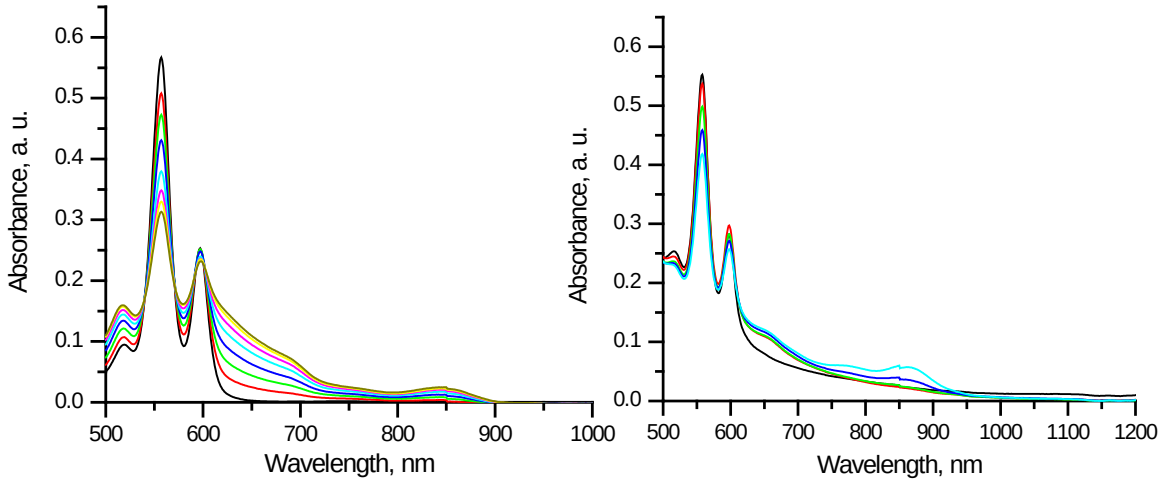

Figure 3.6. Chemical oxidation of porphyrin **1m-Zn** (left) and **1o-Zn** (right) using nitrosonium tetrafluoroborate (0.15 eq. each addition) in methanol.

3.3.2. Photoelectrochemical Studies**.** Figure 3.7 shows the *J-V* characteristics of DSSC employing each of the porphyrin derivatives as photosensitizers under AM1.5 solar illumination conditions. Both working and counter electrodes were sandwiched together, using the thin film TiO_2 as the working electrode and Pt-ized FTO as the counter electrode and employing a solution containing I^-/I_3^- as the redox mediator between the electrode interfaces. In order to avoid dye aggregation, the electrodes were soaked for 4 hr in 0.2 mM dye solution. Losses due to light reflection from the surface of the electrodes have not been corrected. On-off switching experiments were performed, resulting in steady photocurrent in the reported electrodes. The open-circuit potential (V_{oc}), short-circuit current (J_{sc}), fill factor (*FF*), and quantum efficiency (η) for each photosensitizer[114] are reported in Table 3.1. The highest efficiency obtained for the free-base porphyrins was 0.72%, using porphyrin **1m**, which employed both a tolyl substituent and an anchoring group at the *meta* position with respect to the macrocycle. After zinc metallation, the cell under the same experimental conditions showed an increased efficiency, that is, 3.13% for **1p-Zn** and 4.17% for **1m-Zn** were observed. The performance of **1p-Zn** under the

present experimental conditions was slightly lower than that reported earlier by Imahari et. al.[89] In either case, both porphyrins showed an increased efficiency over porphyrins with an *ortho*-carboxylic acid group, porphyrins **1o** and **1o-Zn**. The same trend was seen with the *para* porphyrins with the same substituents (**1p** and **1p-Zn**). When comparing *para* and *meta* derivatized porphyrins, neither seemed to exceed the other when focusing on the same R-groups. Porphyrins bearing propyl alkyl chains and ethylene glycol chains in both *para* (**2p, 2p-Zn, 3m-Zn**) and *meta* (**3m, 3m-Zn 2m, 2m-Zn**) cases showed to be indifferent, suggesting that either orientation is optimal for cell performance. The data in Table 1 also suggests that the better performance of the zinc over free-base porphyrin derivatives is not only due to increased J_{sc} but also due to increased V_{oc} and to some extent due to better fill-factor.

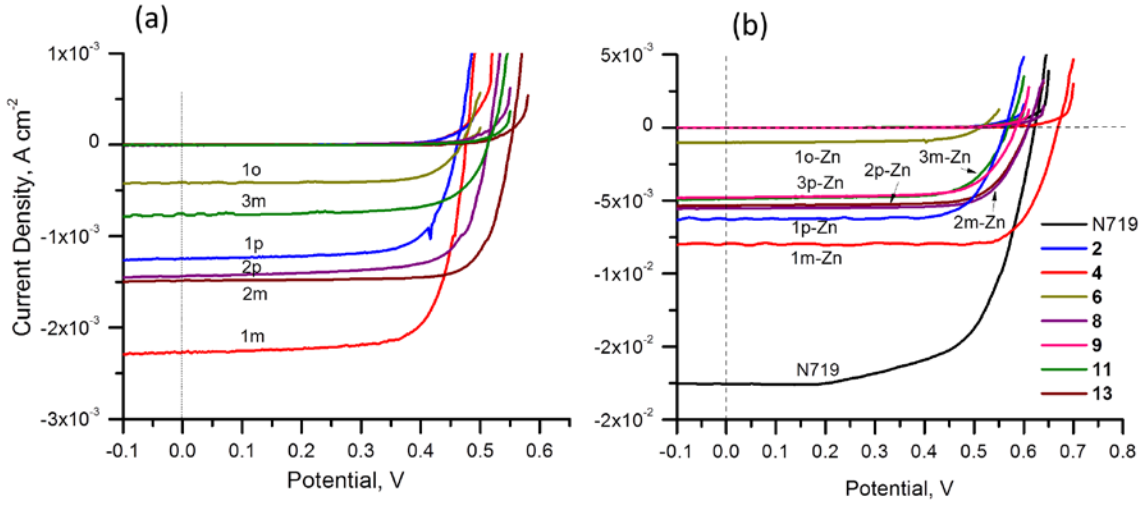

Figure 3.7. Photocurrent density vs. voltage (*J*-*V*) curves of DSSCs built using (a) free-base porphyrin derivatives, and (b) zinc metallated porphyrin derivative as sensitizers under irradiation of AM 1.5G simulated solar light (100 mW cm^{-2}) in the presence of I^-/I_3^- redox mediator (0.6 M propyl methyl iodide (PMII), 0.1 M LiI, 0.05 M I_2, and 0.5 M *ter*-butyl pyridine (TBP)) in acetonitrile.

Table 3.1. Photovoltaic performance[a] of DSSCs based on the synthesized porphyrin derivative dyes with liquid electrolyte.

Dye	J_{sc} (mA/cm^2)	V_{oc} (V)	*FF*	η (%)	Amount (mol/cm^2)
N719	18.13	0.62	0.66	7.39	--
1p	1.26	0.45	0.75	0.42	--
1p-Zn	6.67	0.59	0.79	3.13	1.76×10^{-7}
1m	2.06	0.48	0.72	0.71	--
1m-Zn	8.42	0.65	0.82	4.17	2.19×10^{-7}
1o	0.31	0.45	0.83	0.11	--
1o-Zn	1.01	0.51	0.71	0.37	1.32×10^{-7}
2p	1.17	0.52	0.82	0.65	--
2p-Zn	4.82	0.60	0.77	2.42	--
2m	1.61	0.55	0.74	0.65	--
2m-Zn	5.19	0.61	0.78	2.45	--
3p-Zn	4.88	0.57	0.76	2.09	--
3m	0.78	0.52	0.74	0.30	--
3m-Zn	3.01	0.56	0.73	1.99	--

[a]-average of three DSSCs.

The incident photon-to-current conversion efficiency (IPCE), defined as the number of electrons generated by the light in the outer circuit divided by the number of incident photons, as given by Equation (1):[115]

$$\text{IPCE}(\%) = 100 \times 1240 \times I_{SC}(\text{mA cm}^{-2})/[\lambda(\text{nm}) \times P_{in}(\text{mW cm}^{-2})] \qquad (1)$$

where I_{sc} is the short-circuit current generated by incident monochromatic light illumination and λ is the wavelength of this light at an intensity of P_{in}. The IPCE spectra are shown in Figure 8.

In general, all porphyrins generated appreciable amounts of photocurrent over the range of 350-650 nm for zinc and 350-700 nm range for free-base porphyrins. IPCE performance of N719 DSSC has also been included for reference. Porphyrin **1m-Zn** showed the greatest photocurrent over the region of 500-650 nm, supporting the improved quantum efficiency. Porphyrin **1p-Zn** showed similar IPCE values for the Soret band, but reduced values for the Q bands. As expected, porphyrins **1o** and **1o-Zn** exhibited the lowest IPCE values of the entire group, in agreement with the decreased η values.

The amount of porphyrin adsorbed was calculated by desorbing the adsorbed porphyrin on the TiO_2 surface by the addition of hydroxide for electrodes made out of porphyrins **1p-Zn**, **1m-Zn** and **1o-Zn**. As shown in Table 3.1, the amount of adsorbed dye was slightly higher for **1p-Zn** and **1m-Zn** compared to **1o-Zn**, although all of them were soaked in porphyrin solutions of same concentration (0.2 mM) and same period of time (4 hr). These observations suggest that the flat orientation of adsorbed porphyrin with respect to the TiO_2 surface of the *ortho* derivative (see Figure 3.2) results in slightly less dye intake compared to the *meta* and *para* derivatives.

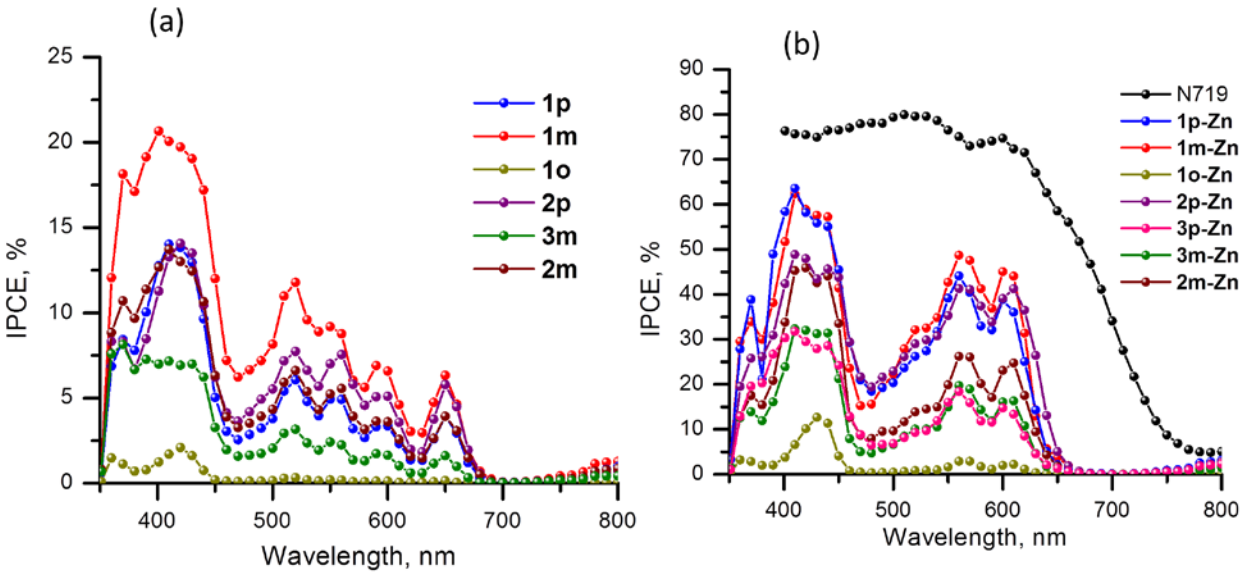

Figure 3.8. Incident photon-to-current conversion action (IPCE %) spectra of mesoporous TiO_2 electrodes sensitized with (a) free-base and (b) zinc metallated porphyrins in acetonitrile containing I^-/I_3^- (0.6 M 1-propyl-3-methylimidazloium iodide (PMII), 0.1 M LiI 0.05 M I_2, and 0.5 M *ter*-butyl pyridine (TBP)) redox mediator using an AM 1.5 simulated light source with a 350 nm UV-cut off filter.

3.3.3. Electrochemical Impedance Spectroscopy Studies. Electrochemical impedance spectroscopy (EIS) studies were performed as this tool is known to be useful in estimating electron recombination resistance and observing the dye regeneration efficiency.[116-117] The Nyquist plots of the free-base porphyrin (Figure 3.9a, b, and c) and zinc porphyrin (Figure 3.9d, e and f) show two semicircles, where the smaller semicircles in high frequency range reflect the charge transfer at the counter electrode/electrolyte interface. While the larger semicircles in the low frequency range correspond to the TiO_2/porphyrin/redox (I^-/I_3^-) electrolyte interface. After analyzing the curves using an equivalent circuit (Figure 3.9 top), the charge transfer resistance of

the counter electrode/electrolyte interface were found to be small under light illumination and dark conditions (Table 3.2). Interestingly, substantially lower R_{ct} were obtained for the TiO_2/porphyrin/redox interface under light illumination compared to the value gathered in dark conditions.

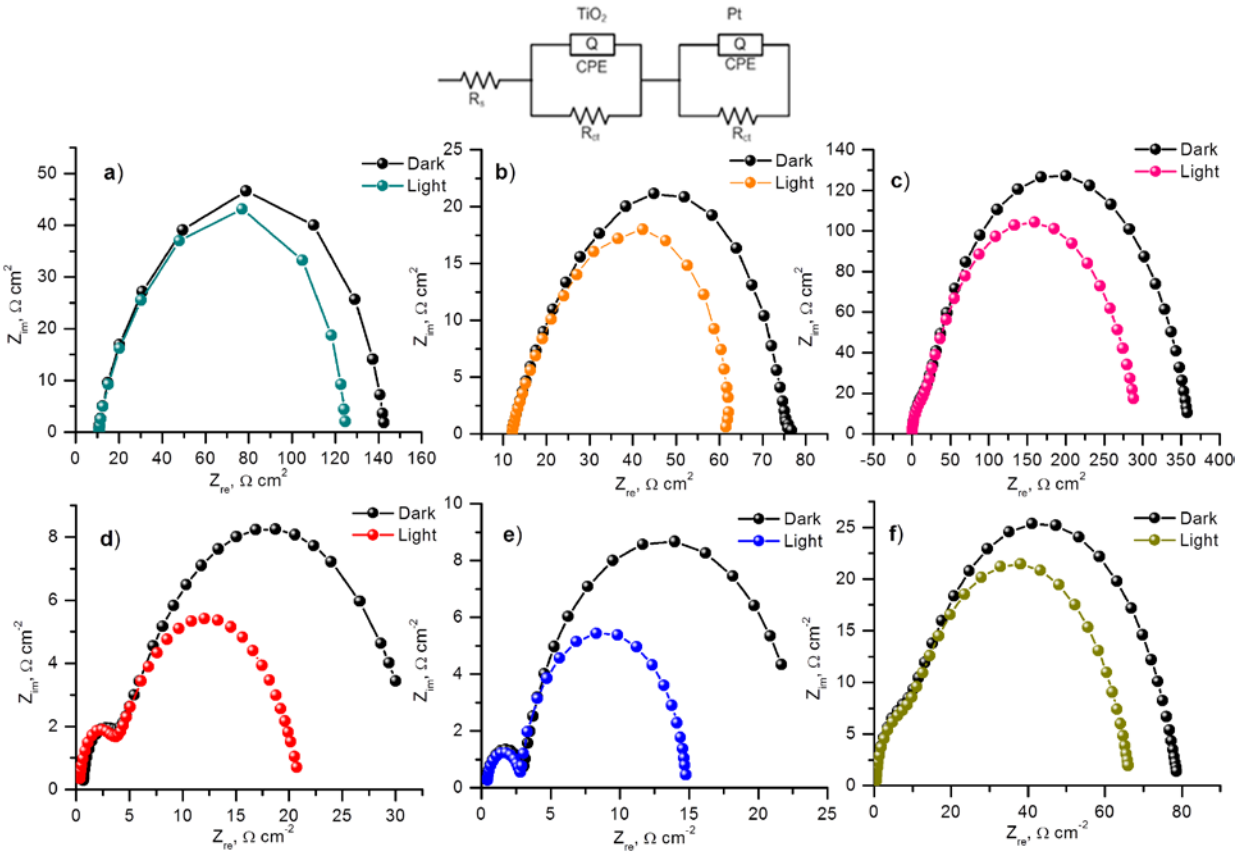

Figure 3.9. Nyquist plots for (a) FTO/TiO_2/**1p**, (b) FTO/TiO_2/**1m**, (c) FTO/TiO_2/**1o**, (d) FTO/TiO_2/**1p-Zn**, (e) FTO/TiO_2/**1m-Zn**, and (f) FTO/TiO_2/**1o-Zn** measured at respective V_{oc} under dark (black line) and AM 1.5 filtered light illumination (colored line) conditions. The figure shown at the top is of the equivalent circuit diagram used to extract the parameters.

Additional observations with respect to the metal ion in the porphyrin cavity and the position of carboxyl group substitution were also made. Generally, a decrease in $R_{ct}(TiO_2)$ can

be attributed to superior photo-regeneration ability which would support an increased efficiency. The observed trend in $R_{ct}(TiO_2)$ for a given series was *meta* < *para* < *ortho*, and zinc porphyrin < free-base porphyrin. The FTO/TiO_2/**1o** showed the greatest charge transfer resistance of 346.9 and 281.0 Ωcm^2, under dark and light conditions respectively. Zinc metallation improved these values to 71.5 and 59.2 Ωcm^2 under dark and light conditions, respectively; however, these values were much higher compared to FTO/TiO_2/**1p-Zn** and FTO/TiO_2/**1m-Zn**. That is, FTO/TiO_2/**1p-Zn** exhibited $R_{ct}(TiO_2)$ values of 29.5 Ωcm^2 under dark conditions and 17.8 Ωcm^2 under AM 1.5 filtered light illumination, whereas, FTO/TiO_2/**1m-Zn** showed reduced R_{ct} values of 20.5 and 12.0 Ωcm^2, under dark and light conditions, respectively. A similar trend was also observed for the free-base porphyrin derivatives (see data in Table 1). These results support the overall lower efficiency of the *ortho* porphyrin derivatives compared to either of *meta* or *para* derivatives.

Table 3.2: Charge transfer resistance values of FTO/TiO_2/porphyrin and counter Pt electrodes (at the respective V_{oc}) estimated using electrochemical impedance spectroscopy.

	$R_{CT}(TiO_2)$ Ωcm^2		$R_{CT}(Pt)$ Ωcm^2	
Dye	dark	light	dark	light
1p	126.9	109.0	11.9	15.5
1p-Zn	29.5	17.8	2.7	3.0
1m	54.1	38.2	5.8	7.7
1m-Zn	20.5	12.0	2.6	2.4
1o	346.9	281.0	14.3	13.4
1o-Zn	71.5	59.2	7.3	7.2

3.3.4. Femtosecond Transient Absorption Spectral Studies. In the present study we have also made an effort to seek a correlation between the orientation induced solar cell efficiency and electron transfer dynamics of the porphyrin modified FTO/TiO_2 electrodes. Zinc porphyrins, **1p-Zn**, **1m-Zn** and **1o-Zn**, representing *para*, *meta* and *ortho* derivatives were employed as they provided the highest energy conversion efficiencies. First, the porphyrins were characterized in solution to get properties of the involved excited states and optimize the spectral region to probe interfacial electron transfer process.

Figure 3.10 shows transient absorption spectra of **1p-Zn** and **1m-Zn** in *o*-dichlorobenzene solution measured at several time intervals after excitation at 400 nm at the Soret region (see supporting information for **1o-Zn**). In agreement with the literature results on femtosecond transient spectra of carboxyl functionalized zinc porphyrin derivatives,[118-119] excitation using 400 nm laser light instantly populated (< 2 ps) the S_2 state of zinc porphyrin with maximum at ~480 nm. At higher wavelength region, two depleted signals at 550 and 588 nm, opposite mimic of the ground state absorption of the Q-bands in Figure 3, were observed. With time, the 588 nm band revealed small red-shift and appeared at 594 nm in the region of Q(0,0) band of steady state emission. The Q(0,1) emission band was also observed at ~668 nm. Collectively, these results point out the occurrence of depleted absorption of the S_0 to S_1 transition and stimulated emission of the S_1 to S_0 state in the transient absorption spectra within the monitored time and spectral window.

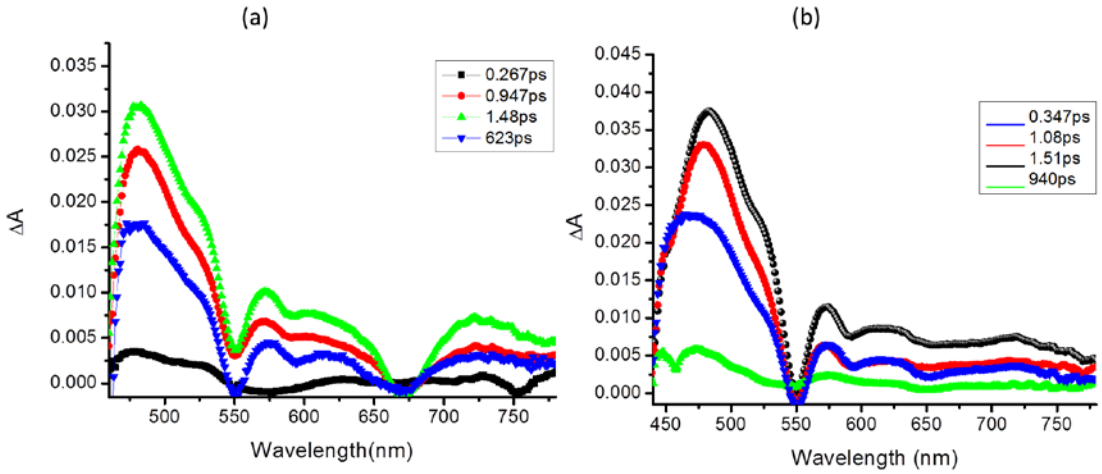

Figure 3.10. Femtosecond transient absorption spectra of (a) **1m-Zn** and (b) **1p-Zn** in *o*-dichlorobenzene at the indicated delay times. The samples were excited with 400 nm femtosecond (100 fs) laser pulses.

Electron injection from surface adsorbed zinc porphyrin to semiconductive TiO_2 would result in the generation of oxidized zinc porphyrin, $ZnP^{\cdot+}$ and reduced TiO_2. Chemical oxidation of compounds **1p-Zn**, **1m-Zn** and **1o-Zn** revealed a relatively strong band at 660 nm and a weaker band at 840 nm as shown in Figure 3.5. Thus, observation of these bands would serve as a diagnostic indication for charge injection, and their rise and decay would provide quantitative information of the kinetics of charge injection and charge recombination. Figures 3.11a and c show transient spectra of FTO/TiO_2/**1m-Zn** and FTO/TiO_2/**1o-Zn** electrodes at different delay times (see Figure 3.12 and 3.13 for FTO/TiO_2/**1p-Zn** spectra). Distinct spectral features from that observed for the pristine zinc porphyrin probe in Figure 10 were observed. A broad band in the 600-700 nm region characteristic of $ZnP^{\cdot+}$ was observed that tracked the S_2 and S_1 states of zinc porphyrin suggesting both these states are involved in charge injection.

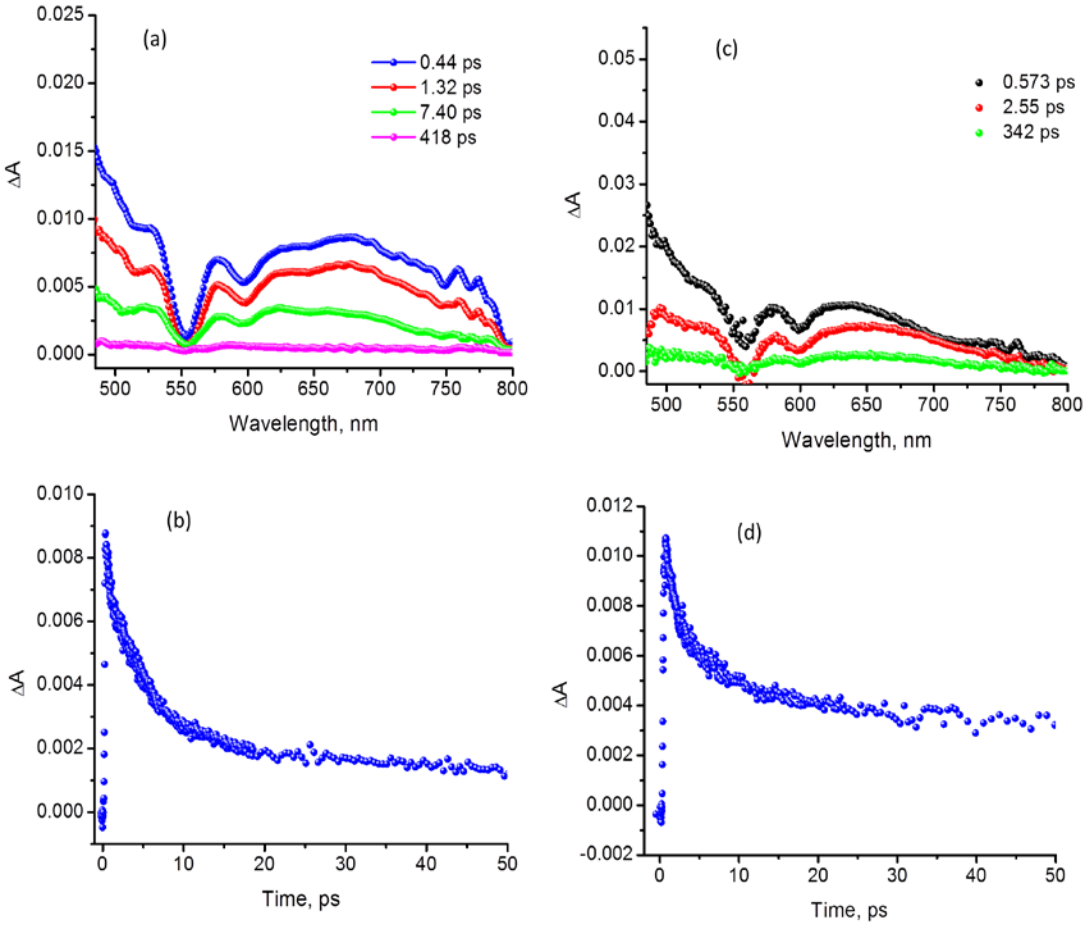

Figure 3.11. Femtosecond transient absorption spectra of (a) FTO/TiO_2/**1m-Zn** and (c) FTO/TiO_2/**1o-Zn** electrodes at the indicated delay times. The samples were excited using 400 nm laser pulses of 100 fs. The time profile of the 660 nm band corresponding to $ZnP^{\cdot+}$ is shown in Figure b and d, respectively, for FTO/TiO_2/**1m-Zn** and FTO/TiO_2/**1o-Zn**.

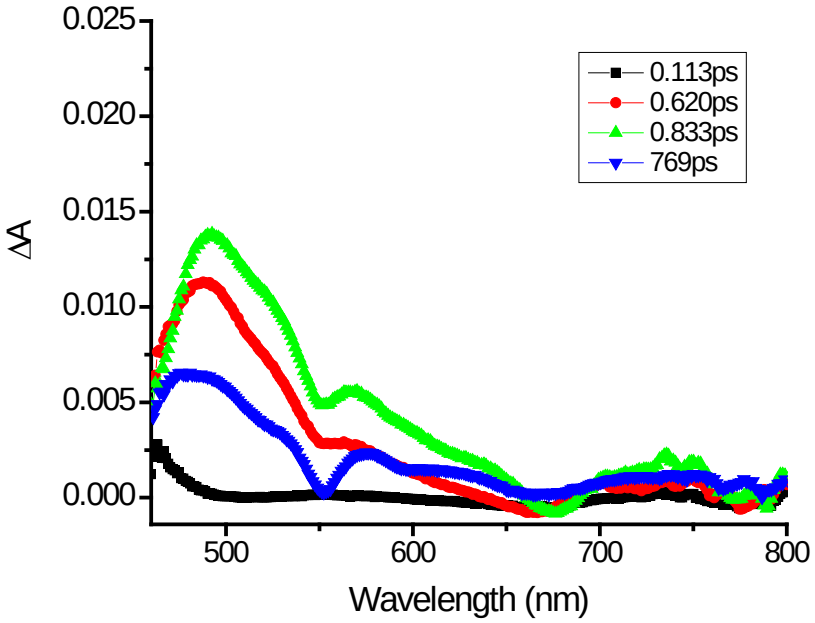

Figure 3.12. Femtosecond transient absorption spectra of **1o-Zn** in *o*-dichlorobenzene at the indicated time delays. The samples were excited 400 nm femtosecond (100 fs) laser pulses.

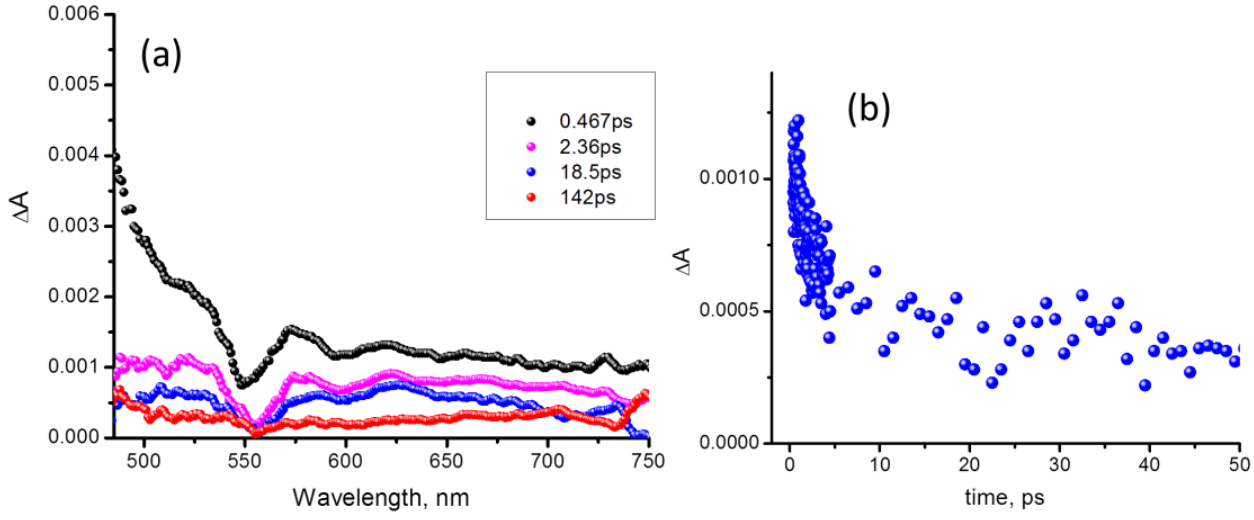

Figure 3.13. Femtosecond transient absorption spectra of FTO/TiO_2/**1p-Zn** electrode at the indicated time delays. The samples were excited using 400 nm laser pulses of 100 fs. The time profile of the 660 nm band corresponding to $ZnP^{\cdot+}$ is shown in Figure b.

Figures 3.11b and d show the time profile of the absorption changes at 660 nm band. The rise was completed within 0.37 to 0.42 ps for all three porphyrin derivatives suggesting ultrafast charge injection. Interestingly, the decay representing the charge recombination lasted for 60-90 ps depending upon the porphyrin isomer and could be fitted to three-exponential fit as shown in Table 3.3. Although for the first two fast decay components it was difficult to see a trend, for the slow decaying major component a clear trend was observed. That is, the charge recombination was much faster for **1o-Zn** compared to **1p-Zn** or **1m-Zn** modified electrodes, perhaps being oriented parallel to the TiO_2 surface.[93]

Table 3.3. Kinetics of charge injection and charge recobmination of FTO/TiO_2:zinc porphyrin electrodes.

Electrode	Rise τ_{av}, ps	Decay τ_1, ps[a]	Decay τ_2, ps[a]	Decay τ_3, ps[a]
FTO/TiO_2:**1p-Zn**	0.30	1.5 (51.2%)	17.8 (21.4%)	88.6 (27.4%)
FTO/TiO_2:**1m-Zn**	0.42	3.5 (59.1%)	10.3 (21.9%)	66.2 (19.0%)
FTO/TiO_2:**1o-Zn**	0.37	1.6 (52.2%)	15.7 (33.1%)	62.7 (14.7%)

[a]-values in parathesis show percent pre-exponential values.

3.4. Discussion

Several interesting observations could be made from the present study that used a relatively simple series of free-base and zinc metallated tetraarylporphyrin derivatives functionalized with a carboxyl group at the *para*, *meta* or *ortho* positions of one of the *meso*-phenyl substituents. The free-base porphyrin derivatives had better spectral coverage in the Q-band region compared to the zinc porphyrin analogs. However, they differed in their oxidation

potentials, that is, the zinc porphyrins were easier to oxidize by about 220 mV compared to free-base porphyrins. It is generally accepted that the carboxyl group binds to the TiO_2 surface as a bidentate ligand using both oxygens.[100-104] This leads to a relatively rigid orientation with respect to the reasonably large suface of TiO_2 (20 nm;18 NRT, Dyesol). Consequently, although fairly close to the surface in all three cases, the estimated macrocycle edge-to-edge distance to the surface of TiO_2 varied as *para* (7-8 Å) > *meta* (5-6 Å) > *ortho* (3-4 Å) (see Figure 2). The alkyl groups on the three aryl rings were also varied to a short methyl group to a medium propyl group to the longer triethyleneoxide groups. While these groups did not significantly purturb either the spectral or redox properties of the porphyrin macrocycle, the long alkyl chains improved the solubility and were expected to reduce the aggregation of porphyrin when immobilized on the TiO_2 surface.

The photoelectrochemical *J-V* plots and IPCE curves revealed the anticipated structure-performance properties. For a given type of porphyrin (*para*, *meta* or *ortho* carboxyl substituent), irrespective of the nature of the alkyl groups, the zinc porphyrins outperformed the free-base porphyrins. Reduced V_{oc} and J_{sc} of free-base porphyrin derived photocells contributed to this cause. The IPCE curves in Figure 3.8 revealed the expected better spectral coverage (350-700 nm) for the free-base porphyrin derived cells compared to zinc porphyrin (300-650 nm) derived cells, however, the former revealed lower IPCE values. In fact, the maximum IPCE observed for **1m** at the Soret region was 23 % which compared with a value of 64% for the zinc porphyrin derivative, **1m-Zn**. The easier to oxidize zinc porphyrin derivatives seem to have a better performance although they revealed less spectral coverage. The presence of long-alkyl chains on porphyrin macrocycle did not necessarily help improve the performance of the photocells, indeed, the best results were obtained for cells made out of tolyl substituents. This

observation suggests that by lowering the dye-adsorption time, one could avoid dye aggregation that would reduce the cell performance. For a given series of *para*, *meta* or *ortho* porphyrin derivaties, the *para* and *meta* derivatives outperformed cells constructed using *ortho* derivatives. It may be mentioned here that the density of the adsorbed dye for the *ortho* porphyrin derivative was slightly lower than the other two (see Table 3.1), although this fact alone could not explain its lower efficiency.

The electrochemical impedance spectroscopic studies of estimation of charge transfer resistance, R_{CT} related to photo-regeneration efficiency of the employed porphyrin sensitizers, and femtosecond transient absorption spectral studies to evaluate kinetics of charge injection and charge recombination from the singlet excited porphyrin to TiO_2 in FTO/TiO_2/porphyrin were useful to further understand the performance of the investigated solar cells. The $R_{CT}(TiO_2)$ values were larger for a given free-base porphyrin compared to its zinc porphyrin analog, in some case by an order of magnitude. Additionally, the *para* and *meta* derivatives revealed the lowest $R_{CT}(TiO_2)$ over the *ortho* derivatives. It has been possible to spectrally characterize the one-electron oxidized product of zinc porphyrin in the wavelength region of 660 nm by femtosecond transient spectroscopic technique. Ultrafast charge injection from singlet excited zinc porphyrin to TiO_2 with a time constant less than 0.42 ps was observed for FTO/TiO_2/zinc porphyrin electrodes. Interestingly, the faster charge recombination in the cases of *ortho* derivative was apparent. This also brings out another important aspect of through-bond and through-space charge transfer.[93] Since all of the derivatives have similar carboxyl linker, any variations in the rates mean contributions from through-space electron transfer in addition to any through-bond contributions. The fast charge recombination in the case of the *ortho* derivative

where the porphyrin macrocycle is much closer to the TiO_2 surface, followed by the *meta* and *para*, is supportive of through-space electron transfer events.

3.5. Summary

In summary, thirteen porphyrin dyes functionalized with a carboxylic acid anchoring group at the *para*, *meta*, or *ortho* positions of one of the phenyl rings of *meso*-tetra aryl porphyrin in addition to varying functional groups of the remaining *meso* positions of the porphyrin ring, were newly synthesized to probe the effect of dye-orientation on TiO_2 surface on their photoelectrochemical performance. Porphyrins were successfully adsorbed onto thin film TiO_2 on FTO and utilized in building DSSCs of two-electrode assembly. The absorption and emission, as well as electrochemical properties were studied to evaluate spectral coverage of free-base and zinc porphyrins as well as their excited state oxidation potentials. It was found that porphyrins anchored to the mesoporous TiO_2 in the *para* and *meta* positions with respect to the porphyrin ring were found to have improved photoelectrochemical properties compared to their *ortho* counterparts. This was supported by femtosecond transient absorption spectroscopy data collected on zinc-metallated porphyrin derivatives, showing fast charge recombination time for the *ortho* derivative adsorbed electrode. Previously, similar porphyrins using multiple anchoring groups were reported by Rochford et al., however, they showed that meta derivatives performed better than para, in this case due to the planar binding of the meta derivatives and aggregation of the para derivative.[101, 103] Similarly, placing tolyl groups in the three remaining *meso* positions showed improved efficiency compared to the long alkyl chain and ethylene oxide groups mentioned in this study. Additionally, the zinc porphyrin derivatives outperformed their free-base porphyrin counterparts. These data are supported by $R_{CT}(TiO_2)$ values, determined from

electrochemical impedance spectral studies, being less for those with zinc at the center of macrocycle cavity. The time-resolved transient absorption studies were also suggestive of occurrence of through-space electron transfer as against through-bond processes.

3.6. Experimental Section

3.6.1. Chemicals. All of the reagents were from Aldrich Chemicals (Milwaukee, WI) while the bulk solvents utilized in the syntheses were from Fischer Chemicals.

3.6.2. Syntheses of free-base porphyrins.[109] In a typical synthesis, 10 mmol of 4-alkyl substituted benzaldehyde, 3.33 mmol of (*o*, *m* or *p*)-formylbenzoic acid and 13.32 mmol of pyrrole were refluxed for 5 hrs in 150 mL of propionic acid. After cooling the mixture at room temperature the solvent was evaporated and the dark black colored crude compound was purified by silica gel column. All the desired compounds were eluted by $CHCl_3$:MeOH (90:10 v/v) and the purity was checked by thin-layer chromatography.

5-(4-Carboxyphenyl)-10,15,20-tris(tolyl)porphyrin, (**1p**)- Yield- 12%. ^{1}H NMR ($CDCl_3$: 400 MHz), δ ppm: −2.45 (s, 2H, −NH), 2.75 (s, 9H, $-CH_3$), 7.55 (d, 6H, phenyl H), 8.10 (dd, 6H, phenyl H), 8.30 (d, 2H, phenyl H), 8.45 (d, 2H, phenyl H), 8.82 (d, 2H, pyrrole), 8.92 (m, 6H, pyrrole H).

5-(3-Carboxyphenyl)-10,15,20-tris(tolyl)porphyrin (**1m**)- Yield- 12.5 %. ^{1}H NMR ($CDCl_3$:400 MHz), δ ppm: -2.81 (s, 2H, -NH), 2.70 (s, 9H, $-3CH_3$), 7.59 (d, 6H, phenyl H), 7.85 (m, 2H, phenyl H), 8.10ppm (d, 6H, phenyl H), 8.40 (d, 1H, phenyl H), 8.50 (d, 1H, phenyl H), 8.80 (m, 2H, pyrrole H), 8.90 (m, 6H, pyrrole H).

5-(2-Carboxyphenyl)-10,15,20-tris(tolyl)porphyrin (**1o**)- Yield- 10.5%. ^{1}H NMR ($CDCl_3$:400 MHz) δ ppm: -2.83 (s, 2H, -NH), 2.62 (s, 9H, $-CH_3$), 7.50 (m, 6H, phenyl H), 7.80

(m, 2H, phenyl H), 8.0 (m, 6H, phenyl H), 8.09 (m, 1H, phenyl H), 8.40 (m, 1H, phenyl H), 8.60 (m, 2H, pyrrole H), 8.80 (m, 6H, pyrrole H).

5-(4-Carboxyphenyl)-10,15,20-tris(4-monomethyl triethyl ether phenoxy)porphyrin (**2p**)- Yield- 11%. ^{1}HNMR ($CDCl_3$:400MHz) δ ppm: -2.83 (s, 2H, -NH), 3.2 (s, 9H, $-CH_3$), 3.45 (m, 6H, $-CH_2$), 3.55 (m, 6H, $-CH_2$), 3.59 (m, 6H, $-CH_2$), 3.65 (m, 6H, $-CH_2$), 3.70 (m, 6H, $-CH_2$), 3.80 (m, 6H, CH_2), 7.20 (dd, 6H, phenyl H), 8.05 (dd, 6H, phenyl H), 8.2 (d, 2H, phenyl H), 8.35 (d, 2H, phenyl H), 8.70 (m, 2H, pyrrole H), 8.80 (m, 2H, pyrrole H).

5-(3-Carboxyphenyl)-10,15,20-tris(4-monomethyl triethyl ether phenoxy)porphyrin (**2m**)- Yield- 10%. ^{1}HNMR ($CDCl_3$:400 MHz), δ ppm: -2.86 (s, 2H, -NH), 3.35 (s, 9H, $-CH_3$), 3.55 (m, 6H, $-CH_2$), 3.62 (m, 6H, $-CH_2$), 3.70 (m, 6H, $-CH_2$), 3.80 (m, 6H, $-CH_2$), 3.95 (m, 6H, $-CH_2$), 4.35 (m, 6H, CH_2) 7.20 (d, 6H, phenyl H), 7.79 (t, 1H, phenyl H), 7.90 (d, 1H, phenyl H), 8.05 (d, 6H, phenyl H), 8.32 (d, 1H, phenyl H), 8.40 (d, 1H, phenyl H), 8.75 (m, 2H, pyrrole H), 8.81 (m, pyrrole H).

5-(3-Carboxyphenyl)-10,15,20-tris(4-propylphenyl)porphyrin (**3m**)- Yield- 14%. ^{1}HNMR ($CDCl_3$:400 MHz), δ ppm: -2.85 (s, 2H, -NH), 1.10 (m, 9H, $-CH_3$), 1.60 (m, 6H, $-CH_2$), 1.95 (m, 6H, $-6H_2$), 7.50 (d, 6H, phenyl H), 7.77 (t, 1H, phenyl H), 7.90 (d, 1H, phenyl H), 8.05 (d, 6H, phenyl H), 8.35 (d, 1H, phenyl H), 8.42 (d, 1H, phenyl H), 8.75 (m, 2H, pyrrole H), 8.85 (m, 6H, pyrrole H).

3.6.3. Synthesis of zinc porphyrins.[110] In a typical experiment, free-base porphyrin (90 mg) and zinc acetate (1:5 mol ratio) were refluxed in chloroform and methanol (1:1 ratio, 10 mL each) until free-base porphyrin was completely metalated which was checked by the UV−vis spectrum which showed disappearance of the 515 nm band. After evaporation of solvent, the crude

compound was purified over silica gel column, and the desired compound was eluted by chloroform:methanol (95:5 v/v).

[5-(4-Carboxyphenyl)-10,15,20-tris(tolyl)porphyrinato]zinc(II) (**1p-Zn**)- Yield- 85%. ^{1}H NMR ($CDCl_3$: 400 MHz), δ ppm: 2.70 (s, 9H, $-CH_3$), 7.60 (d, 6H, phenyl H), 8.15 (dd, 6H, phenyl H), 8.25 (d, 2H, phenyl H), 8.45 (d, 2H, phenyl H), 8.85 (d, 2H, pyrrole), 8.95 (m, 6H, pyrrole H).

[5-(3-Carboxyphenyl)-10,15,20-tris(tolyl)porphyrinato]zinc(II) (**1m-Zn**)- Yield- 87%. ^{1}H NMR ($CDCl_3$:400 MHz), δ ppm: 2.60 (s, 9H, $-3CH_3$), 7.45 (d, 6H, phenyl H), 7.78 (m, 2H, phenyl H), 8.01 (d, 6H, phenyl H), 8.30 (d, 1H, phenyl H), 8.43 (d, 1H, phenyl H), 8.70 (m, 2H, pyrrole H), 8.81 (m, 6H, pyrrole H).

[5-(2-Carboxyphenyl)-10,15,20-tris(tolyl)porphyrinato]zinc(II) (**1o-Zn**) – Yield- 80%. ^{1}HNMR ($CDCl_3$:400 MHz) δ ppm: 2.60 (s, 9H, $-CH_3$), 7.42 (m, 6H, phenyl H), 7.79 (m, 2H, phenyl H), 8.0 (m, 6H, phenyl H), 8.10 (m, 1H, phenyl H), 8.35 (m, 1H, phenyl H), 8.60 (m, 2H, pyrrole H), 8.79 (m, 6H, pyrrole H).

[5-(4-Carboxyphenyl)-10,15,20-tris(4-phenyl monomethyl ethyl ether)porphyrinato] zinc(II) (**2p-Zn**)- Yield- 78%. ^{1}HNMR ($CDCl_3$:400 MHz) δ ppm: 3.35 (s, 9H, $-CH_3$), 3.49 (m, 6H, $-CH_2$), 3.55 (m, 6H, $-CH_2$), 3.62 (m, 6H, $-CH_2$), 3.70 (m, 6H, $-CH_2$), 4.10 (m, 6H, $-CH_2$), 6.85 (dd, 6H, phenyl H), 7.92 (dd, 6H, phenyl H), 8.21 (m, 2H, phenyl H), 8.38 (m, 2H, phenyl H), 8.75 (m, 2H, pyrrole H), 8.82 (m, 6H, pyrrole H).

[5-(4-Carboxyphenyl)-10,15,20-tris(4-propylphenyl)porphyrinato]zinc(II) (**3p-Zn**) – Yield 85%. ^{1}HNMR ($CDCl_3$:400 MHz), δ ppm: 1.20 (m, 9H, $-CH_3$), 1.65 (m, 6H, $-CH_2$), 1.95 (m, 6H, $-CH_2$),), 7.60 (d, 6H, phenyl H), 8.15 (dd, 6H, phenyl H), 8.35 (d, 2H, phenyl H), 8.40 (d, 2H, phenyl H), 8.85 (d, 2H, pyrrole), 8.95 (m, 6H, pyrrole H).

[5-(3-Carboxyphenyl)-10,15,20-tris(4-propylphenyl)porphyrinato]zinc(II) (**3m-Zn**). Yield- 77%. ^{1}H NMR ($CDCl_3$:400 MHz), δ ppm: 0.95 (m, 9H, -CH_3), 1.30 (m, 6H, -CH_3), 1.95 (m, 6H, -CH_2), 7.45 (d, 6H, phenyl H), 7.78 (m, 2H, phenyl H), 8.05 (d, 6H, phenyl H), 8.38 (m, 2H), 8.70 (m, 2H, pyrrole H), 8.81 (m, 6H, pyrrole H).

[5-(3-Carboxyphenyl)-10,15,20-tris(4-phenyl monomethyl ethyl ether)porphyrinato] zinc(II) (**2m-Zn**). Yield- 76%. ^{1}H NMR ($CDCl_3$:400 MHz), δ ppm: 3.27 (s, 9H, -CH_3), 3.50 (m, 12H, -CH_2), 3.57 (m, 6H, -CH_2), 3.61 (m, 6H, -CH_2), 3.72 (m, 6H, -CH_2), 4.25 (m, 6H, -CH_2), 7.12 (d, 6H, phenyl H), 7.70 (t, 1H, phenyl H), 7.85 (d, 1H, phenyl H), 7.95 (d, 6H, phenyl H), 8.30 (m, 2H, phenyl H), 8.68 (m, 2H, pyrrole H), 8.79 (m, 6H, pyrrole H).

3.6.4. Spectral Measurements. The UV-visible measurements were collected either using a Jasco V-670 spectrophotometer or a Shimadzu Model 2550 double monochromator UV-visible spectrophotometer. The steady state fluorescence spectra were measured using a Horiba Jobin Yvon Nanolog UV-visible-NIR spectrofluorometer equipped with a PMT (for UV-visible) and InGaAs (for NIR) detectors. The ^{1}H NMR studies were carried out on a Bruker 400 MHz spectrometer. Tetramethylsilane (TMS) was used as an internal standard. Differential pulse voltammograms were recorded on an EG&G 263A potentiostat/galvanostat using a three electrode system. A platinum button electrode was used as the working electrode, while a platinum wire served as the counter electrode and an Ag/AgCl electrode was used as the reference electrode. Ferrocene/ferrocenium redox couple was used as an internal standard. All the solutions were purged prior to electrochemical and spectral measurements with nitrogen gas.

3.6.5. Photoelectrochemical Measurements. Photoelectrochemical measurements were performed using the Grätzel-type two-electrode system using FTO (~10-12 microns, tec7 grade from Pilkington) glass coated with thin film TiO_2 as the working electrode and Pt-ized FTO as

the counter electrode. The thin film TiO_2 was prepared *via* the "Doctor blade" technique as reported earlier.[80] A mediator solution containing 0.1 M LiI, 0.05 M I_2, and 0.5 M 4-*t*-butylpyridine in acetonitrile was injected between the electrodes.

The photocurrent-photovoltage characteristics were collected using a Keithley Instruments Inc. (Cleveland, OH) Model 2400 Current/Voltage Source Meter under illumination from a simulated light source using a Model 9600 of 150-W Solar Simulator of Newport Corp. (Irvine, CA) and filtered using an AM 1.5 filter. Incident photon-to-current efficiency (IPCE) measurements were performed under ~4 mW cm^2 monochromatic light illumination conditions using a setup comprised of a 150 W Xe lamp with a Cornerstone 260 monochromator (Newport Corp., Irvine, CA).

3.6.6. Electrochemical Impedance Measurements. Electrochemical impedance measurements were performed using EG&G PARSTAT 2273 potentiostat/galvanostat. Impedance data were recorded under forward bias condition from 100 kHz to 50 mHz with an AC amplitude of 10 mV. Data were recorded under dark and A.M 1.5 illumination conditions applying corresponding open circuit potential (V_{oc}). The data were analyzed using ZSimpwin software from Princeton Applied Research. Solution resistance (R_s), charge transfer resistance (R_{ct}), and capacitance due to constant phase element (Q) were deduced from the fitted data. CPE was considered as capacitance component of the double layer electrode interface due to roughness of the electrode.

3.6.7. Femtosecond Transient Absorption Spectral Measurements. Femtosecond transient absorption spectroscopy experiments were performed using an Ultrafast Femtosecond Laser Source (Libra) by Coherent incorporating diode-pumped, mode locked Ti:Sapphire laser (Vitesse) and diode-pumped intra cavity doubled Nd:YLF laser (Evolution) to generate a compressed laser output of 1.45 W. For optical detection a Helios transient absorption

spectrometer coupled with femtosecond harmonics generator both provided by Ultrafast Systems LLC was used. The source for the pump and probe pulses were derived from the fundamental output of Libra (Compressed output 1.45 W, pulse width 91 fs) at a repetition rate of 1 kHz. 95% of the fundamental output of the laser was introduced into harmonic generator which produces second and third harmonics of 400 nm and 267 nm besides the fundamental 800 nm for excitation, while the rest of the output was used for generation of white light continuum. In the present study, the second harmonic 400 nm excitation pump was used in all the experiments. Kinetic traces at appropriate wavelengths were assembled from the time-resolved spectral data. All measurements were conducted at 298 K.

3.6.8. Preparation of Electrodes for Photoelectrochemical and Transient Studies. Electrodes were prepared by cleaning FTO by sonicating individually in solutions of 0.1 M HCl, acetone, and isopropanol. Next, the FTO was allowed to soak in 20 mM solution of $TiCl_4$ at 70° C for 30 minutes. Then, a layer of 20 nm anatase TiO_2 (18 NRT, Dyesol) was applied on the surface of the FTO using the doctor blade technique and allowed to dry in air for 20 minutes. The FTO/TiO_2 was then annealed in a heat cycle of 130° C, 230° C, 330° C, 390° C, 440° C, and 515° C for 10 minutes each. After cooling, a second layer of 20 nm anatase TiO_2 was applied and annealed in a similar fashion. Next, the electrodes were allowed to soak in a fresh $TiCl_4$ solution for an additional 30 minutes at 70° C. Then the films were annealed at 440° C for 30 minutes and then cooled at 130° C before immersing in 0.2 mM sensitizer solution for 4 hours.

3.7. References

1. O'Regan B.; Grätzel, M. *Nature*, **1991**, *353*, 737.
2. Grätzel, M. *Nature* **2001**, *414*, 338.

3. Nazeeruddin, M. K.; Pechy, P.; Renouard, T.; Zakeeruddin, S. M.; Humphry-Baker, R.; Comte, P.; Liska, P.; Cevey, L.; Costa, E.; Shklover, V.; Spiccia, L.; Deacon, G. B.; Bignozzi, C. A.; Grätzel, M. *J. Am. Chem. Soc*. **2001**, *123*, 1613.

4. Nazeeruddin, M. K.; De Angelis, F.; Fantacci, S.; Selloni, A.; Viscardi, G.; Liska, P.; Ito, S.; Bessho, T.; Grätzel, M. *J. Am. Chem. Soc*. **2005**, *127*, 16835.

5. Chiba, Y.; Islam, A.; Watanabe, Y.; Komiya, R.; Koide, N.; Han, L. Y. Jpn. *J. Appl. Phys*. **2006**, *45*, L638.

6. Nazeeruddin, M. K.; Bessho, T.; Cevey, L.; Ito, S.; Klein, C.; De Angelis, F.; Fantacci, S.; Comte, P.; Liska, P.; Imai, H.; Grätzel, M.A *J. Photochem. Photobiol. A* **2007**, *185*, 331.

7. (g) Gao, F.; Wang, Y.; Shi, D.; Zhang, J.; Wang, M. K.; Jing, X. Y.; Humphry-Baker, R.; Wang, P.; Zakeeruddin, S. M.; Grätzel, M. *J. Am. Chem. Soc*. **2008**, *130*, 10720.

8. Chen, C. Y.; Wang, M. K.; Li, J. Y.; Pootrakulchote, N.; Alibabaei, L.; Ngoc-le, C. H.; Decoppet, J. D.; Tsai, J. H.; Gratzel, C.; Wu, C. G.; Zakeeruddin, S. M.; Grätzel, M. *ACS Nano* **2009**, *3*, 3103.

9. Hagfeldt, A.; Boschloo, G.; Sun, L.; Kloo, L.; Pettersson, H. *Chem. Rev*. **2010**, *110*, 6595.

10. Cao, Y. M.; Bai, Y.; Yu, Q. J.; Cheng, Y. M.; Liu, S.; Shi, D.; Gao, F. F.; Wang, P. *J. Phys. Chem. C* **2009**, *113*, 6290.

11. Han, L. Y.; Islam, A.; Chen, H.; Malapaka, C.; Chiranjeevi, B.; Zhang, S. F.; Yang, X. D.; Yanagida, M. *Energy Environ. Sci*. **2012**, *5*, 6057.

12. Moser, J. E.; Bonnote, P.; Grätzel, M. Coord. *Chem. Rev*. **1998**, *171*, 245.

13. Robertson, N. *Angew. Chem., Int. Ed.* **2006**, *45*, 2338.

14. Pelet, S.; Grätzel, M.; Moser, J. E. *J. Phys. Chem. B* **2003**, *107*, 3215.

15. Haque, S. A.; Tachibana, Y.; Willis, R. L.; Moser, J. E.; Grätzel, M.; Klug, D. R.; Durrant, J. R. *J. Phys. Chem. B* **2000**, *104*, 538.

16. Chen, C.; Wang, M.; Wang, K. *J. Phys. Chem. C* **2009**, *113*, 1624.

17. Myllyperkio, P.; Manzoni, C.; Polli, D.; Cerullo, G.; Korppi-Tommola, J. *J. Phys. Chem. C* **2009**, *113*, 13985.

18. Wiberg, J.; Marinado, T.; Hagberg, D. P.; Sun, L. C.; Hagfeldt, A.; Albinsson, B. *J. Phys. Chem. C* **2009**, *113*, 3881.

19. Ravirajan, P.; Peiró, A. M.; Nazeeruddin, M. K.; Grätzel, M.; Bradley, D. D. C.; Durrant, J. R.; Nelson, J. *J. Phys. Chem. B* **2006**, *110*, 7635.

20. Anderson, S.; Constable, E. C.; Dareedwards, M. P.; Goodenough, J. B.; Hamnett, A.; Seddon, K. R.; Wright, R. D. *Nature* **1979**, *280*, 571.

21. Tachibana, Y.; Moser, J. E.; Grätzel, M.; Klug, D. R.; Durrant, J. R. *J. Phys. Chem*. **1996**, *100*, 20056.

22. Hannappel, T.; Burfeindt, B.; Storck, W.; Willig, F. *J. Phys. Chem. B* **1997**, *101*, 6799.

23. Moser, J. E.; Noukakis, D.; Bach, U.; Tachibana, Y.; Klug, D. R.; Durrant, J. R.; Humphry-Baker, R.; Grätzel, M. *J. Phys. Chem. B* **1998**, *102*, 3649.

24. Ellingson, R. J.; Asbury, J. B.; Ferrere, S.; Ghosh, H. N.; Sprague, J. R.; Lian, T. Q.; Nozik, A. J. *J. Phys. Chem. B* **1998**, *102*, 6455.

25. Asbury, J. B.; Ellingson, R. J.; Ghosh, H. N.; Ferrere, S.; Nozik, A. J.; Lian, T. Q. *J. Phys. Chem. B* **1999**, *103*, 3110.

26. Durrant, J. R.; Tachibana, Y.; Mercer, I.; Moser, J. E.; Grätzel, M.; Klug, D. R. Z. *Phys. Chem*. **1999**, *212*, 93.

27. Tachibana, Y.; Haque, S. A.; Mercer, I. P.; Durrant, J. R.; Klug, D. R. *J. Phys. Chem. B* **2000**, *104*, 1198.

28. Haque, S. A.; Handa, S.; Peter, K.; Palomares, E.; Thelakkat, M.; Durrant, J. R. *Angew. Chem., Int. Ed*. **2005**, *44*, 5740.

29. Nelson, J.; Haque, S. A.; Klug, D. R.; Durrant, J. R. *Phys. Rev. B* **2001**, *63*, 205321.

30. Heimer, T. A.; Heilweil, E. J.; Bignozzi, C. A.; Meyer, G. J. *J. Phys. Chem. A* **2000**, *104*, 4256.

31. Kallioinen, J.; Lehtovuori, V.; Myllyperkio, P.; Korppi-Tommola, J. *Chem. Phys. Lett*. **2001**, *340*, 217.

32. Benko, G.; Kallioinen, J.; Korppi-Tommola, J. E. I.; Yartsev, A. P.; Sundström, V. *J. Am. Chem. Soc*. **2002**, *124*, 489.

33. Kallioinen, J.; Benko, G.; Sundström, V.; Korppi-Tommola, J. E. I.; Yartsev, A. P. *J. Phys. Chem. B* **2002**, *106*, 4396.

34. Anderson, N. A.; Lian, T. *Coord. Chem. Rev*. **2004**, *248*, 1231.

35. Schwarzburg, K.; Ernstorfer, R.; Felber, S.; Willig, F. *Coord. Chem. Rev*. **2004**, *248*, 1259.

36. Barzykin, A. V.; Tachiya, M. *J. Phys. Chem. B* **2002**, 106, 4356.

37. Katoh, R.; Furube, A.; Barzykin, A. V.; Arakawa, H.; Tachiya, M. *Coord. Chem. Rev.* **2004**, *248*, 1195.

38. Barzykin, A. V.; Tachiya, M. *J. Phys. Chem. B* **2004**, *108*, 8385.

39. Pan, J.; Benko, G.; Xu, Y. H.; Pascher, T.; Sun, L. C.; Sundström, V.; Polivka, T. *J. Am. Chem. Soc.* **2002**, *124*, 13949.

40. Wang, D.; Mendelsohn, R.; Galoppini, E.; Hoertz, P. G.; Carlisle, R. A.; Meyer, G. J. *J. Phys. Chem. B* **2004**, *108*, 16642.

41. Kilsa, K.; Mayo, E. I.; Kuciauskas, D.; Villahermosa, R.; Lewis, N. S.; Winkler, J. R.; Gray, H. B. *J. Phys. Chem. A* **2003**, *107*, 3379.

42. Tian, H. N.; Yang, X. C.; Cong, J. Y.; Chen, R. K.; Liu, J.; Hao, Y.; Hagfeldt, A.; Sun, L. *C. Chem. Commun*. **2009**, 6288.

43. Wang, Z. S.; Koumura, N.; Cui, Y.; Miyashita, M.; Mori, S.; Hara, K. *Chem. Mater*. **2009**, *21*, 2810.

44. Qin, H.; Wenger, S.; Xu, M.; Gao, F.; Jing, X.; Wang, P.; Zakeeruddin, S. M.; Grätzel, M. *J. Am. Chem. Soc*. **2008**, *130*, 9202.

45. Zhou, G.; Pschirer, N.; Schoneboom, J. C.; Eickemeyer, F.; Baumgarten, M.; Mullen, K. *Chem. Mater*. **2008**, *20*, 1808.

46. Xu, W.; Peng, B.; Chen, J.; Liang, M.; Cai, F. *J. Phys. Chem. C* **2008**, *112*, 874.

47. Li, G.; Jiang, K.-J.; Li, Y.-F.; Li, S.-L.; Yang, L.-M. *J. Phys. Chem. C* **2008**, *112*, 11591

48. Ning, Z. J.; Zhang, Q.; Wu, W. J.; Pei, H. C.; Liu, B.; Tian, H. *J. Org. Chem*. **2008**, *73*, 3791.

49. Horiuchi, T.; Miura, H.; Sumioka, K.; Uchida, S. *J. Am. Chem. Soc*. **2004**, *126*, 12218.

50. Zhang, X. H.; Wang, Z. S.; Cui, Y.; Koumura, N.; Furube, A.; Hara, K. *J. Phys. Chem. C* **2009**, *113*, 13409.

51. Hara, K.; Sayama, K.; Ohga, Y.; Shinpo, A.; Suga, S.; Arakawa, H.A *Chem. Commun*. **2001**, 569.

52. Wang, Z. S.; Cui, Y.; Dan-Oh, Y.; Kasada, C.; Shinpo, A.; Hara, K. *J. Phys. Chem. C* **2007**, *111*, 7224.

53. Wang, Z. S.; Cui, Y.; Dan-Oh, Y.; Kasada, C.; Shinpo, A.; Hara, K. *J. Phys. Chem. C* **2008**, *112*, 17011.

54. Horiuchi, T.; Miura, H.; Uchida, S. *Chem. Commun*. **2003**, 3036.

55. Hara, K.; Kurashige, M.; Ito, S.; Shinpo, A.; Suga, S.; Sayama, K.; Arakawa, H. *Chem. Commun*. **2003**, 252.

56. Kitamura, T.; Ikeda, M.; Shigaki, K.; Inoue, T.; Anderson, N. A.; Ai, X.; Lian, T. Q.; Yanagida, S. *Chem. Mater*. **2004**, *16*, 1806.

57. Hwang, S.; Lee, J. H.; Park, C.; Lee, H.; Kim, C.; Park, C.; Lee, M.-H.; Lee, W.; Park, J.; Kim, K.; Park, N.-G.; Kim, C.A *Chem. Commun*. **2007**, 4887.

58. Kim, C.; Choi, H.; Kim, S.; Baik, C.; Song, K.; Kang, M. S.; Kang, S. O.; Ko, J. *J. Org. Chem*. **2008**, *73*, 7072.

59. Im, H.; Kim, S.; Park, C.; Jang, S. H.; Kim, C. J.; Kim, K.; Park, N. G.; Kim, *C. Chem. Commun*. **2010**, *46*, 1335.

60. Tan, S. X.; Zhai, J.; Fang, H. J.; Jiu, T. G.; Ge, J.; Li, Y. L.; Jiang, L.; Zhu, D. B. *Chem.—Eur. J*. **2005**, *11*, 6272.

61. Liu, W. H.; Wu, I. C.; Lai, C. H.; Chou, P. T.; Li, Y. T.; Chen, C. L.; Hsu, Y. Y.; Chi, Y. *Chem. Commun*. **2008**, 5152.

62. Wang, Z. S.; Koumura, N.; Cui, Y.; Takahashi, M.; Sekiguchi, H.; Mori, A.; Kubo, T.; Furube, A.; Hara, K. *Chem. Mater*. **2008**, *20*, 3993.

63. Wu, W. J.; Hua, J. L.; Jin, Y. H.; Zhan, W. H.; Tian, H. *Photochem. Photobiol. Sci.* **2008**, *7*, 63.

64. Yum, J. H.; Walter, P.; Huber, S.; Rentsch, D.; Geiger, T.; Nuesch, F.; De Angelis, F.; Grätzel, M.; Nazeeruddin, M. K. *J. Am. Chem. Soc*. **2007**, *129*, 10320.

65. Reddy, P. Y.; Giribabu, L.; Lyness, C.; Snaith, H. J.; Vijaykumar, C.; Chandrasekharan, M.; Lakshmikantam, M.; Yum, J. H.; Kalyanasundaram, K.; Grätzel, M.; Nazeeruddin, M. K. *Angew. Chem., Int. Ed*. **2007**, *46*, 373.

66. Cid, J. J.; Yum, J. H.; Jang, S. R.; Nazeeruddin, M. K.; Ferrero, E. M.; Palomares, E.; Ko, J.; Grätzel, M.; Torres, T. *Angew. Chem., Int. Ed*. **2007**, *46*, 8358.

67. Martinez-Diaz, M. V.; de la Torre, G.; Torres, T. *Chem. Commun*. **2010**, *46*, 7090.

68. Mori, S.; Nagata, M.; Nakahata, Y.; Yasuta, K.; Goto, R.; Kimura, M.; Taya, M. *J. Am. Chem. Soc*. **2010**, *132*, 4054.

69. Ragoussi, M. E.; Cid, J. J.; Yum, J. H.; de la Torre, G.; Di Censo, D.; Grätzel, M.; Nazeeruddin, M. K.; Torres, T. *Angew. Chem., Int. Ed*. **2012**, *51*, 4375.

70. Ferrere, S.; Zaban, A.; Gregg, B. A. *J. Phys. Chem. B* **1997**, *101*, 4490.

71. Shibano, Y.; Umeyama, T.; Matano, Y.; Imahori, H. *Org. Lett*. **2007**, *9*, 1971.

72. Li, C.; Yum, J. H.; Moon, S. J.; Herrmann, A.; Eickemeyer, F.; Pschirer, N. G.; Erk, P.; Schoeboom, J.; Mullen, K.; Grätzel, M.; Nazeeruddin, M. K. *ChemSusChem* **2008**, *1*, 615.

73. Mathew, S.; Imahori, H.Tunable, *J. Mater. Chem*. **2011**, *21*, 7166.

74. Zhang, G. L.; Bala, H.; Cheng, Y. M.; Shi, D.; Lv, X. J.; Yu, Q. J.; Wang, P. *Chem. Commun*. **2009**, 2198.

75. Zeng, W. D.; Cao, Y. M.; Bai, Y.; Wang, Y. H.; Shi, Y. S.; Zhang, M.; Wang, F. F.; Pan, C. Y.; Wang, P. *Chem. Mater*. **2010**, *22*, 1915.

76. Tian, H.; Yang, X.; Chen, R.; Pan, Y.; Li, L.; Hagfeldt, A.; Sun, L. *Chem. Commun.*, **2007**, 3741.

77. Cao, D.; Peng, J.; Hong, Y.; Fang, X.; Wang, L.; Meier, H. *Org. Lett.*, **2011**, *13*, 1610.

78. Xie, Z.; Midya, A.; Loh, K. P.; Adams, S.; Blackwood, D. J.; Wang, J.; Zhang, X.; Chen, Z. *Prog. Photovoltaics*, **2010**, *18*, 573.

79. Wu, W.; Yang, J.; Hua, J.; Tang, J.; Zhang, L.; Long, Y.; Tian, H. *J. Mater. Chem.*, **2010**, *20*, 1772.

80. Hart A.S.; KC C. B.; Subbaiyan N. K.; Karr P. A.; D'Souza F. *ACS Appl. Mater. Inter.*, **2012** *4*, 5813.

81. Sargent, E. H.; *Nature Photonics*, **2012**, *6*, 133.

82. Bang, J. H.; Kamat, P. V. *ACS Nano*, **2009**, *3*, 1467.

83. Tang, J.; Wang, X.; Brzozowski, L.; Barkhouse, D.; Aaron, R.; Debnath, R.; Levina, L.; Sargent, E. H. *Adv. Mater*. **2010**, *22*, 1398.

84. Wang, Q.; Campbell, W. M.; Bonfantani, E. E.; Jolley, K. W.; Officer, D. L.; Walsh, P. J.; Gordon, K.; Humphry-Baker, R.; Nazeeruddin, M. K.; Grätzel, M. *J. Phys. Chem. B* **2005**, *109*, 15397.

85. Campbell, W. M.; Jolley, K. W.; Wagner, P.; Wagner, K.; Walsh, P. J.; Gordon, K. C.; Schmidt-Mende, L.; Nazeeruddin, M. K.; Wang, Q.; Grätzel, M.; Officer, D. L. *J. Phys. Chem. C* **2007**, *111*, 11760.

86. Lee, C. Y.; She, C. X.; Jeong, N. C.; Hupp, J. T. *Chem. Commun*. **2010**, *46*, 6090.

87. Imahori, H.; Umeyama, T.; Ito, S. *Acc. Chem. Res*. **2009**, *42*, 1809.

88. Walter, M. G.; Rudine, A. B.; Wamser, C. C. *J. Porphyrins Phthalocyanines* **2010**, *14*, 759.

89. Imahori, H.; Matsubara, Y.; Iijima, H.; Umeyama, T.; Matano, Y.; Ito, S.; Niemi, M.; Tkachenko, N. V.; Lemmetyinen, H. *J. Phys. Chem. C* **2010**, *114*, 10656.

90. Kira, A.; Matsubara, Y.; Iijima, H.; Umeyama, T.; Matano, Y.; Ito, S.; Niemi, M.; Tkachenko, N. V.; Lemmetyinen, H.; Imahori, H. *J. Phys. Chem. C* **2010**, *114*, 11293.

91. Mathew, S.; Iijima, H.; Toude, Y.; Umeyama, T.; Matano, Y.; Ito, S.; Tkachenko, N. V.; Lemmetyinen, H.; Imahori, H. *J. Phys. Chem. C* **2011**, *115*, 14415.

92. Imahori, H.; Umeyama, T.; Kurotobi, K.; Takano, Y. *Chem. Commun*. **2012**, *48*, 4032.

93. Ye, S.; Kathiravan, A.; Hayashi, H.; Tong, Y.; Infahsaeng, Y.; Chabera, P.; Pascher, T.; Yartsev, A. P.; Isoka, S.; Imahori, H.; Sundström, V. *J. Phys. Chem*. **2013**, *117*, 6066.

94. Subbaiyan, N. K.; Wijesinghe, C. A.; D'Souza, F. *J. Am. Chem. Soc*., **2009**, *131*, 14646.

95. Hasobe, T. *Phys. Chem. Chem. Phys.*, **2010**, *12*, 44.

96. Ishida, M.; Park, S. W.; Hwang, D.; Koo, Y. B.; Sessler, J. L.; Kim, D. Y.; Kim, D. *J. Phys. Chem. C* **2011**, *115*, 19343.

97. Wang, F.; Subbaiyan, N. K.; Wang, Q.; Rochford, C.; Xu, G.; Lu, R.; Elliot, A.; D'Souza, F.; Hut, R.; Wu, J. *ACS Appl. Mater. Interfaces* **2012**, *4*, 1565.

98. KC, C. B.; Stranius, K.; D'Souza, P.; Subbaiyan, N. K.; Lemmetyinen, H.; Tkachenko, N. V.; D'Souza, F. *J. Phys. Chem. C*. **2013**, *117*, 763.

99. Subbaiyan, N. K.; Hill, J. P.; Ariga, K.; Fukuzumi, S.; D'Souza, F. *Chem. Commun*. **2011**, *47*, 6003.

100. Cherian, S.; Wamser, C. C. *J. Phys. Chem. B* **2000**, *104*, 3624.

101. Rochford, J.; Chu, D.; Hagfeldt, A.; Galoppini, E. *J. Am. Chem. Soc.* **2007**, *129*, 4655.

102. Rangan, S.; Katallinic, S.; Thorpe, R.; Bartynski, R. A.; Rochford, J.; Galoppini, E. *J. Phys.Chem. C* **2010**, *114*, 1139.

103. Rochford, J.; Galoppini, E. *Langmuir*, **2008**, *24*, 5366.

104. Ma, T. L.; Inoue, K.; Noma, H.; Yao, K.; Abe, E. *J. Photochem. Photobiol. A: Chem*. **2002**, *152*, 207

105. Bessho, T.; Zakeeruddin, S. M.; Yeh, C. Y.; Diau, E. W. G.; Grätzel, M. *Angew. Chem., Int. Ed*. **2010**, *49*, 6646.

106. Wang, C. L.; Chang, Y. C.; Lan, C. M.; Lo, C. F.; Diau, E. W. G.; Lin, C. Y. *Energy Environ. Sci*. **2011**, *4*, 1788.

107. Chang, Y. C.; Wang, C. L.; Pan, T. Y.; Hong, S. H.; Lan, C. M.; Kuo, H. H.; Lo, C. F.; Hsu, H. Y.; Lin, C. Y.; Diau, E. W. *Chem. Commun*. **2011**, *47*, 8910.

108. Yella, A.; Lee, H. W.; Tsao, H. N.; Yi, C. Y.; Chandiran, A. K.; Nazeeruddin, M. K.; Diau, E. W. G.; Yeh, C. Y.; Zakeeruddin, S. M.; Grätzel, M. *Science* **2011**, *334*, 629.

109. Kim, J. B.; Adler, A. D.; Long, F. R. In *The Porphyrins*; Dolphin, D., Ed.; Academic Press: New York, 1978, Vol. IA, pp 85-100.

110. Smith, K. M. *Porphyrins and Metalloporphyrins*; Elsevier: Amsterdam 1972, pp 798.

111. Gouterman, M. *J. Mol. Spectrosc*. **1961**, *6*, 138-163.

112. McHugh, A. J.; Gouterman, M.; Weiss, C. Jr. *Theor. Chim. Acta* **1972**, *24*, 346-70.

113. Kadish, K. M. *Prog. Inorg. Chem*. **1986**, *34*: 435.

114. *Dye-Sensitized Solar Cells*; Kalyanasundaram, K. Ed.; EPFL Press: Lausanne, 2010.

115. Hasobe, T; Saito, K; Kamat, P.V.; Troiani, V; Qui, H; Solladie, N; Kim, K.S.; Park, J.K.; Kim, D; D'Souza, F; Fukuzumi, S. *J. Mater. Chem*. **2007**, *17*, 4160.

116. Bisquert, J; Fabregat-Santiago, F. In *Dye-Sensitized Solar Cells*; Kalyanasundaram, K., Ed.; EPFL Press: Lausanne, Switzerland, 2010; Chapter 12, pp 457-554.

117. Subbaiyan, NK; Maligaspe, E; D'Souza, F. *ACS Appl. Mater. Interfaces* **2011**, *3*, 2368.

118. Chang, C.-W.; Luo, L.; Chou, C.-K.; Lo, C.-F.; Lin, C.-Y.; Hung, C.-S.; Lee, Y.-P.; Kiau, E. W. G. *J. Phys. Chem. C*. **2009**, *113*, 11524.

119. Imahori, H.; Kang, S.; Hayashi, H.; Haruta, M.; Kurata, H.; Isoda, S.; Canton, S.; Infahsaeng, Y.; Kathiravan, A.; Pascher, T.; Chábera, P.; Yartsev, A.; Sundström, V. *J. Phys. Chem. A* **2011**, *115*, 3679.

CHAPTER 4

SUMMARY

In summary, the details of dye sensitized solar cells was explained and phenothiazine and porphyrin based dyes were synthesized for use in DSSCs. DSSCs offer a unique and cost effective method of renewable energy. DSSCs can be best described in terms of their individual components: the absorbed dye sensitizer, the oxide film substrate, the counter electrode, and the redox mediator solution. In DSSCs, energy is generated by the flow of electrons from the dye sensitizer to the oxide film layer, then to the output destination. In turn, the electrons must also flow back through the counter electrode and into the redox mediator solution, which then replenishes the dye sensitizer. However, thermodynamics and current losses prevent this from being a fully efficient process. The conditions in which these individual parts are made can help limit these losses. Specifics in ways to improve each component were discussed to give further insight on how they work. DSSCs are characterized through various tests, with the overall efficiency, η, bearing the greatest importance. The efficiency of DSSCs depends on the individual characteristics: open circuit potential, V_{oc}, the short-circuit current, I_{sc}, and fill factor, *FF*; each of which is described in more detail in the first chapter. Incident photon to current conversion efficiency, or *IPCE*, is also another important characterization of DSSCs. This characteristic is a measure of how much current is generated by the cell at individual wavelengths and can show how well the device performs under the UV-visible regions of light.

In the second chapter, phenothiazine derivative dyes were probed based on substitution effects and the positioning of the anchoring position of the dye for use in DSSCs. Four phenothiazine dyes functionalized with a cyanoacrylic acid group either directly at the macrocycle carbon (Type-1) or via macrocycle N-atom (Type-2) were studied and characterized.

Type-1 dyes were shown to have a much greater overall efficient than the Type-2 dye, with **3** exhibiting the greatest efficiency at 4.07%. Similarly, Type-1 dyes showed IPCE values extending across more of the visible region of the light spectrum than the Type-2 dye. These conclusions were supported using fluorescence lifetime studies, electrochemical impedance spectroscopy (EIS), and electrochemical studies. Additionally, computational studies showed further insight into the differences in the LUMO levels between Type-2 and Type-1 dyes and how this has contributed to the results.

In chapter 3, substitution effects and anchoring group positioning was examined by constructing DSSCs. Thirteen porphyrin dyes functionalized with a carboxylic acid anchoring group at the *para*, *meta*, or *ortho* positions of one of the phenyl rings of porphyrin and varying functional groups of the remaining meso positions of the porphyrin ring, and employed in DSSCs to probe the effect of dye-orientation on TiO_2 substrate to evaluate their performance. Studies showed that dyes with the anchoring group in the *ortho* position were much less efficient than their *meta* and *para* counterparts. Similarly, zinc-metallation increased the efficiency of the dyes as compared to their free-base hydrogen counterparts. Sensitizer **1m-Zn** showed the greatest photoelectrochemical properties, with an efficiency of 4.17%. These conclusions were supported using EIS studies, electrochemical studies, and femtosecond transient spectroscopy studies, for the zinc derivatives.